NASA TECHNICAL MEMORANDUM

NASA TM X-2096

NASA TM X-2096

CENTAUR - ORBITING ASTRONOMICAL OBSERVATORY NOSE FAIRING ALTITUDE JETTISON TEST

by Charles W. Eastwood

Lewis Research Center
Cleveland, Ohio 44135

NATIONAL AERONAUTICS AND SPACE ADMINISTRATION • WASHINGTON, D. C. • SEPTEMBER 1970

1. Report No. NASA TM X-2096	2. Government Accession No.	3. Recipient's Catalog No.
4. Title and Subtitle CENTAUR - ORBITING ASTRONOMICAL OBSERVATORY NOSE FAIRING ALTITUDE JETTISON TEST		5. Report Date September 1970 6. Performing Organization Code
7. Author(s) Charles W. Eastwood		8. Performing Organization Report No. E-5673
9. Performing Organization Name and Address Lewis Research Center National Aeronautics and Space Administration Cleveland, Ohio 44135		10. Work Unit No. 491-01 11. Contract or Grant No. 13. Type of Report and Period Covered Technical Memorandum
12. Sponsoring Agency Name and Address National Aeronautics and Space Administration Washington, D.C. 20546		14. Sponsoring Agency Code
15. Supplementary Notes		

16. Abstract

An experimental investigation was conducted to verify the functional and structural capability of the Centaur - OAO-A2 nose fairing at the jettison altitude predicted for the first Centaur-OAO flight. A full-scale fairing specimen was exposed to the simulated atmospheric pressure associated with the flight jettison event. Three complete jettisons of the fairing were performed, one with the redundant separation system disabled. Nose fairing specimen trajectories, structural deflections, clearances, hinge forces, and shock loads in the simulated pressure environment are presented. Several subsystem component parameters were established and are presented. Data from the subsequent Centaur-OAO flight are compared with the experimental results.

17. Key Words (Suggested by Author(s))	18. Distribution Statement
Nose fairing Altitude jettison test Nose fairing hinge loads Fairing jettison deflections Fairing spacecraft clearance	Unclassified - unlimited

19. Security Classif. (of this report)	20. Security Classif. (of this page)	21. No. of Pages	22. Price*
Unclassified	Unclassified	61	$3.00

*For sale by the Clearinghouse for Federal Scientific and Technical Information
Springfield, Virginia 22151

CENTAUR - ORBITING ASTRONOMICAL OBSERVATORY NOSE FAIRING ALTITUDE JETTISON TEST

by Charles W. Eastwood
Lewis Research Center

SUMMARY

The Atlas-Centaur aerospace vehicle employs a jettisonable nose fairing to encapsulate and protect the Orbiting Astronomical Observatory (OAO) spacecraft from aerodynamic forces during ascent through the earth's atmosphere. When the vehicle has attained an altitude above the denser atmosphere, the clamshell-type fairing is jettisoned from the second-stage Centaur. This event separates the fairing weight from the second stage, as well as deencapsulating the spacecraft preparatory to later spacecraft separation from the vehicle. In order to verify the structural integrity of the fairing and the functional capability of the separation system at altitude, an experimental investigation was conducted at the Lewis Research Center. A flight-type nose fairing assembly encapsulating an OAO spacecraft inertial model was subjected to the simulated flight pressure environment in a vacuum chamber. Vehicle axial acceleration was not exactly duplicated; the earth's 1-g surface gravity was used as a simulation of the 0.8 g experienced at fairing jettison. The fairing separation system was activated and the nose fairing was jettisoned from a mockup of the Centaur forward end. Catch nets were utilized to decelerate and capture the fairing halves. Three jettison tests were performed. The final test was conducted with the pyrotechnic separation system redundant initiators and one jettison actuator inoperative.

Each of the test runs was successful in demonstrating the structural and functional capability of the nose fairing system during jettison. The structural integrity of the specimen was maintained without failure. Separation and jettison characteristics of the fairing halves at the predicted rates were verified.

All pyrotechnic detonators in the latching mechanisms fired, including the sympathetic firing of the disconnected redundant electroexplosive devices in the third test. Fairing trajectories and clearances were within the design limits. The hinge load data indicated acceptable levels of force transfer into the supporting fixed fairing section. Fairing structural deflections during the jettison event were as predicted. Data related to trajectories, dynamic characteristics, hinge loads, clearances, and spacecraft shock loads from each of the tests are presented. The results of several secondary investigations, (1) separation friction force, (2) fairing rocking clearance losses, (3) J-ring structural deflection, (4) radiographic determination of spacecraft static clearance after encapsulation, are also presented. It was determined from the experimental investigation that all components and subsystems of the nose fairing in the flight configuration were suitable for their required functions.

INTRODUCTION

A nose fairing 3.05 meters (10 ft) in diameter by 12.27 meters (40.23 ft) long, including the 9.72-meter (31.89-ft) long jettisonable section, is used with the Atlas-Centaur vehicle that launches the Orbiting Astronomical Observatory (OAO) into earth orbit (fig. 1). The fairing is a low-drag cylindrical-to-conical configured lightweight shell assembled from fiber glass and metallic sections. It is mounted on the forward end of the Centaur stage and encapsulates the payload and the forward-mounted vehicle equipment. The primary function of the fairing is to minimize the aerodynamic forces on the vehicle and to completely protect the spacecraft and vehicle equipment from these forces during ascent through the atmosphere. At an altitude of approximately 270 kilometers (150 n mi), sufficiently above the effects of the denser atmosphere, the jettisonable bisegment section of the fairing is jettisoned from the Centaur vehicle. This event is performed (1) to eliminate the weight of the functionally expended fairing and (2) to deencapsulate the OAO spacecraft in preparation for OAO separation from Centaur at the appropriate flight time. It is essential, of course, that the fairing jettison be successfully accomplished in order to place the OAO in orbit. Therefore, the separation system must unlatch the fairing halves and jettison them clear of the vehicle. Simultaneously, the fairing halves must retain their structural integrity while subjected to the jettison forces.

The nose fairing is a composite of existing and new designs. It incorporates the existing design of the fairing separation system and the basic nose cone section of the Atlas-Agena vehicle that was used to launch the first OAO spacecraft. Also, it includes the existing design of the cylindrical aft section of the Centaur-Surveyor nose fairing. Two other cylindrical sections are of new design. The existing designs have many modifications incorporated for adaptation to the Centaur-OAO requirements. A configuration outline of the nose fairing, indicating new and existing designs and the modifications thereto, is shown in figure 2.

Analysis of the design indicated that the fairing would perform satisfactorily at jettison. The calculated fairing separation forces, structural capabilities, dynamic characteristics, hardware clearances, and jettison trajectories were adequate for the established requirements. Component designs incorporated from other vehicle fairings had been previously evaluated and verified by ground testing and flight usage during their development. However, the component redesigns, which were incorporated for adaptation to the Centaur-OAO fairing, reduced the effective use of the earlier experimental conclusions in evaluating the new application. In addition, the combination of several component designs into a composite fairing design precluded the correlation of most of the existing full-scale test data. Since a satisfactory fairing jettison is required for a successful mission, verification of the design and analysis by functional testing of

the complete fairing assembly was necessary to establish confidence for flight use. Therefore, a test program was initiated to qualify the composite design.

The primary objective of the test program was to verify the structural integrity and functional capability of the nose fairing system during jettison at simulated altitude. The secondary objective was to determine that parametric values of the fairing system characteristics were within design limits. An additional purpose of the program was to substantiate several component parameters and a radiographic clearance measuring technique by conducting subsystem tests.

Valuable assistance was provided by the fairing contractor, Convair Division of General Dynamics Corporation, during the entire test program.

TEST PROGRAM

The overall objective of the development test program was to qualify the fairing system for flight use. Test conditions specified that a prototype flight fairing specimen be used, that an inertial mass model of the OAO spacecraft be included, and that the tests be performed in a simulated atmospheric pressure equivalent to at least 27 432 meters (90 000 ft) of altitude. Also, the specimen was to be tested in a vertical position to employ the 1-g surface gravity of the earth as the gross equivalent of the 0.8 g axial accceleration of the vehicle at fairing jettison. Other environmental parameters of flight such as ambient temperature, vehicle vibration, and lateral motion were not duplicated.

Primary objectives were as follows:

(1) To successfully perform two successive jettison tests of the complete fairing system for verification of the functional and structural capability of the fairing and separation system and to establish repeatability

(2) To successfully perform a jettison test with one of the two separation actuators inoperative and one of the dual sets of pyrotechnic initiators in the separation latches disconnected from the firing circuit for functional verification of the system redundancy

Successful jettison was defined in the program as follows: (1) all pyrotechnics must fire within 10 milliseconds after application of firing voltage, (2) all jettisonable hardware must separate cleanly, and (3) functional or structural failures must not occur.

Secondary objectives of the test program were to substantiate the following:

(1) Fairing jettison trajectories

(2) Fairing structural deflections during jettison

(3) Fairing-spacecraft dynamic clearances

(4) Fairing hinge loads during jettison

(5) Thermal bulkhead dynamic clearances

(6) Shock loads transferred to the spacecraft during fairing jettison

In addition to the fairing jettison tests, the program included a series of subsystem tests. The subsystem test objectives were to experimentally determine the following:

(1) Capability of the barrel section to support the fairing-spacecraft static load with access doors opened in prescribed sequence

(2) Clearance loss from fairing rocking dynamics

(3) Fairing split line shear pin maximum acceptable mismatch

(4) Technique for measuring the fairing-spacecraft static clearance by X-ray photography

(5) Deflection and spring rate of the payload adapter support ring (J-ring)

NOSE FAIRING CONFIGURATION

Nose Fairing Description

The nose fairing is a 3.05-meter (10-ft) diameter cylindrical shell terminating in a cone at the forward end. It consists of a 2.55-meter (8.34-ft) long nonjettisonable section, which is bolted to the Centaur vehicle forward mounting ring, and a 9.72-meter (31.89-ft) long jettisonable section that is attached to the nonjettisonable section of the assembly (fig. 2). The nonjettisonable portion consists of a 1.86-meter (6.09-ft) long cylindrical barrel section and a 0.69-meter (2.25-ft) long cylindrical fixed fairing section. A wide ring with a J section configuration is sandwiched between the fixed fairing and the barrel sections to support the spacecraft adapter and the thermal bulkhead. The jettisonable portion of the fairing is a bolted assembly of a 0.90-meter (2.96-ft) long split fairing and an 8.82-meter (28.93-ft) long cylindrical-to-conical nose cone section.

A split line divides the jettisonable portion into two longitudinal halves, except for the cap at the forward tip that is attached to the quadrant II-III half of the fairing. Each of the jettisonable fairing halves has two hinge fittings at the aft end that assemble to mating fittings on the fixed fairing. Blast shields extend along the inboard edge of the -X longeron on the quadrant II-III fairing half and the +X longeron on quadrant I-IV half to deflect any leakage of ram air from impinging on the spacecraft during vehicle ascent. Inside the jettisonable fairing is an annular-shaped encapsulation bulkhead that is mounted approximately 1.14 meters (45 in.) forward of the aft end. A flexible rubber seal on the inner diameter of the bulkhead connects to the spacecraft mounting adapter. The bulkhead and seal isolate the payload compartment in the nose cone section for environmental control of the spacecraft. Six dual-function vent valves are mounted in the bulkhead to regulate the compartment pressure during launch preparation by means of spring-loaded poppets in the valves. At vehicle launch the main flappers in the valves are opened to vent the payload compartment atmospheric pressure through

the equipment compartment and finally overboard through the vent ports in the barrel section during flight ascent.

The jettisonable fairing weight, including all equipment, is 1115 kilograms (2459 lbm). The quadrant II-III fairing half, which has the cap, weighs 587 kilograms (1295 lbm) and quadrant I-IV 528 kilograms (1164 lbm).

The barrel and nose cone sections are of phenolic - glass-fiber sandwich construction. Material thicknesses and nose fairing dimensions are shown in figure 3. Glass-fabric-reinforced plastic honeycomb constitutes the core with inner and outer skin laminates of phenolic resin - glass cloth. A layer of sheet cork is bonded to the outer skin of the nose cone section to dissipate the aerodynamic heating. The cork limits temperature of the phenolic resin adhesives in order to maintain fairing structural integrity. The barrel section is surfaced with a layer of a subliming heat-absorbing material for the same reason. Both the fixed fairing section and the split fairing section are of metallic construction. They are fabricated from aluminum inner framing rings, skin, and outer stringers.

The longitudinal bisegmented jettisonable portion of the fairing is joined together by 10 latch mechanisms, five on each side of the fairing, spaced along the separation split line. At the aft separation plane, six latches on the inner periphery fasten the assembly to the fixed fairing. Pins positioned along the separation seams impart shear load capability to the assembly. The latches are released at the time of jettison by pyrotechnic operation of piston-actuated split-nut and bolt devices within the mechanisms. A programmed signal from the launch vehicle activates fairing-mounted control relays. The relays, in turn, direct power from jettison system batteries to the pyrotechnic cartridges. Each pyrotechnic cartridge is detonated by an electrically heated bridgewire that is in contact with the heat-sensitive explosive charge. Two complete pyrotechnic subsystems are used. Each subsystem consists of a battery, two relay assemblies, and 16 electroexplosive cartridges. Although one cartridge will operate a latch adequately, each of the 16 latch mechanisms are operated by two cartridges, one from each subsystem, for system redundancy. The forces to accomplish fairing jettison are applied by two preloaded compression spring actuator assemblies mounted in the forward end, one in each fairing half. Each actuator has a retracted length of 73.7 centimeters (29 in.), a stroke of 72.4 centimeters (28.5 in.), and a spring rate of 7375 newtons per meter (42.5 lb/in.). The spring preload is 5493 newtons (1235 lbf) for each actuator. One spring actuator will furnish sufficient energy to jettison the fairing, with two being used to raise the level of functional reliability. Upon issuance of the jettison command signal by the Centaur programmer, the relay assemblies mounted in the fairings electrically complete the circuits from the fairing-mounted batteries to the pyrotechnic cartridges. At release of the separation latches, the energy furnished by the spring actuators forces the fairing halves to rotate outboard on the aft-mounted hinges. The hinges are a fork-and-pivot-pin design that permits hinge disengagement and separation after the first 30^{o}

of rotation. Fairing design is such, however, that the forces during jettison will separate the fairings from the vehicle hinges at approximately 70^{o} of fairing rotation.

Test Article Description

One test article was used for the three jettison tests that were performed. Expendables, such as the electroexplosive cartridges in the separation latches, were replaced for each test run. All components of the test article were flight configuration, except for some details which were not pertinent. The weight of the test jettisonable fairing without the cork covering was 1061 kilograms (2340 lbm); quadrant II-III fairing half weighed 556 kilograms (1226 lbm) and quadrant I-IV 505 kilograms (1114 lbm).

The nose cone section was an existing assembly that formerly had been used in the Agena-OAO nose fairing jettison test program. Modifications were incorporated (fig. 2) to update the section to conform to the Centaur-OAO configuration as follows:

(1) The ground service air conditioning inlet was relocated 99 centimeters (39 in.) aft from the conical area to a location on the cylindrical area.

(2) An access door 43 centimeters (17 in.) in diameter was incorporated near the aft end of the section.

(3) The annular-shaped encapsulation bulkhead was relocated 2.90 centimeters (1.14 in.) aft, and the inner diameter was increased 7.62 centimeters (3.0 in.) to 2.45 meters (96.5 in.).

(4) In place of the full-length blast shields which were not on the test fairing, 61-centimeter (24-in.) long sections were installed in the critical clearance area on both longerons of the quadrant II-III fairing half.

The cork thermal covering was not included on the test specimen because of the anticipated high incidence of mechanical damage to the cork by the catcher equipment. A mass simulation of the cork was not added because its effect on the jettison characteristics of the fairing is negligible.

For the test program, only one of the six vent valves was installed in the encapsulation bulkhead since the test chamber pumpdown was much too slow for evaluation of the venting capacity of the valves. Therefore, only a functional check of the valve flapper opening and latching operation before start of test was planned, and a single vent valve sufficed.

The split fairing section was a newly fabricated flight item. Since its design is peculiar to the Centaur-OAO, no modifications were required. Similarly, the fixed fairing section was a new flight item of Centaur-OAO peculiar design and incorporated no modifications.

An existing Centaur-Surveyor-type barrel section was partially modified for use as a component of the test article. The forward structural ring was replaced with a ring

member of Centaur-OAO design. Two load-bearing struts of nonflight design were incorporated in the umbilical cutout area to simulate the design capability of the OAO-type umbilical panel. Other structural modifications such as the additional fiber-glass skin plies and the heavier-weight core material at the forward and aft ends of the section, to react the flight loads, were not incorporated as only the fairing jettison loads were to be experienced during the test. Analytical and experimental verification of the structural capability of the barrel section had been previously accomplished in a separate study and test program. The 5° vent fairing was not installed on the test article.

In addition to the basic nose fairing shell, the test article included a 1927-kilogram (4248-lbm) inertial model spacecraft which duplicated the flight configuration. The following payload support components were included: conical adapter, cylindrical adapter, and spacecraft adapter (fig. 2). The conical adapter was an existing Agena-OAO component that was slightly modified to update it to the Centaur-OAO configuration. The cylindrical adapter was a metallic mockup with equivalent basic dimensions and approximately equivalent dynamic characteristics. The spacecraft adapter was an existing prototype assembly and the spacecraft was a dimensionally accurate, inertial model.

As part of the test article, the quadrant II-III half of the bisegmented thermal bulkhead and new-design supporting struts were included. A minor modification was incorporated into the outer-diameter attachment hardware to conform to the Centaur-OAO configuration (fig. 2).

Flight-type instrumentation pertinent to the fairing jettison event was included as a component system of the test article. Each fairing half utilized one electrical disconnect and two breakwire transducers as fairing rotation position indicators. The four aft hinge arms (two per fairing half) were strain gaged for sensing the axial and radial loads transmitted to the fixed fairing during the jettison event. A more detailed description of these instruments is given in the section TEST FACILITY: Instrumentation and Data Recording.

TEST FACILITY

Structure and Equipment

Testing was performed in the Space Power Chamber facility of NASA Lewis Research Center. The facility consists of an operations building and an attached steel structure that houses two altitude test chambers. The tests were conducted in the center section (test area) of test chamber 2, as shown in figure 4. Essentially, this part of the chamber is a large, steel, horizontal cylinder with an inside diameter of 15.5 meters (51 ft) and a length of 36.9 meters (121 ft). Chamber 2 has a total volume of 16 400 cubic meters (185 000 ft^3). It is connected to a large-capacity pumping system

capable of reducing the chamber internal pressure to the equivalent of an altitude of 30.5 kilometers (100 000 ft) in approximately 1 hour of pumpdown time. Facility services available within the chamber are area lighting, electrical power, compressed air, and monorail-mounted hoists. An annular-shaped platform elevator with an inside diameter of 3.35 meters (11 ft) was installed in the center of the test area. This service platform could be elevated on guide columns to any level between the floor and ceiling of the test chamber for ready accessibility to the 14.5-meter (47.5-ft) high test article during erection and servicing.

Within the center opening of the annular-shaped service elevator a steel test base 3.05 meters (10 ft) in diameter was leveled and welded to the chamber floor. A cylindrical metal shell 3.05 meters (10 ft) in diameter and 130 centimeters (51.2 in.) high, capable of adequately withstanding the test article static and jettison loads, was bolted to the base as a spacer. On the upper flange of the spacer, a simulated Centaur forward bulkhead was installed. It consisted of a steel frame with a 0.95-centimeter (3/8-in.) thick fiber-glass skin contoured to the dimensions of the Centaur forward bulkhead, including the forward 30.5 centimeters (12 in.) of the Centaur cylindrical tank. At vehicle equivalent station 219, a flight-type forward tank ring was bolted onto the simulated bulkhead. The base, spacer, and simulated bulkhead assembly served as a mounting platform for the fairing and payload test article.

In order to decelerate and arrest the motion of the jettisoned fairing halves, a catcher and snubber system was installed in the test area. Two 15.2-meter (50-ft) long by 9.1-meter (30-ft) wide nylon nets (0.6-cm (1/4-in.) cord netted into 7.6-cm (3-in.) mesh) were supported approximately 3.35 meters (11 ft) above the chamber floor to catch and decelerate the fairing halves after each jettison, as shown in figure 5. To prevent excessive rebound of the fairings, each net had 12 snubber assemblies. Each assembly consisted of a rope bridle attached to the underside of the net, snubbed around a floor-mounted drum, and pretensioned with an elastic-cord takeup line.

Plan, elevation, and sectional views of the test chamber and test support equipment arrangement are shown in figure 6.

In addition to the general area lighting and the electrically operated hoists, electrical power was used for motion-picture-camera operation and floodlighting. Standard 110-volt alternating current was used to power both systems. The floodlighting was operated by manual switch from the facility control room. Motion-picture cameras were energized through an automatic switch operated by a test event sequencer located in the control room.

The control system consisted of the event sequencer and an event timer. The sequencer was programmed to initiate three events: (1) switch on the cameras and the oscillograph recorders prior to start of the test, (2) furnish a command signal to the event timer to start the test, and (3) switch off the cameras and recorders at test termination. The first event was initiated immediately following activation of the

sequencer. Time-delay relays in the sequencer initiated the second event 3 seconds later and the third event 13 seconds after sequencer start.

The event timer issued pulse signals to camera timing lights and to the oscillograph and magnetic tape recorders for correlation of data. The pulses were $16\frac{2}{3}$ milliseconds in duration at 100-millisecond intervals. An isolation circuit in the timer restrained the pulses from being issued prior to the start of the test. Upon receipt of the command signal from the sequencer, a holding circuit in the event timer restrained the signal until the next timing pulse was generated. At that instant the command signal and the timing pulses were related simultaneously to the nose fairing jettison control unit and to the recorders and timing lights, respectively. A block diagram of the control system is shown in figure 7.

Instrumentation and Data Recording

Electrical transducers, mechanical sensors, and high-speed motion-picture cameras were used to measure the various events during test. Table I is a tabulation of all instruments and recorders employed in the test series.

Of the four types of electrical transducers used, three were of flight configuration. They were (1) breakwire type, (2) electrical bus disconnect type, and (3) strain gage type. The lanyard-operated breakwire transducers were located at the hinge line and indicated the 15° and 45° angular position event times of the fairing halves during jettison. The bus disconnects were specific circuits that terminated in electrical system connectors located at the jettison hardware interface. Rotation of the fairing halves operated mechanical lanyards that caused the connectors to separate and to open the circuits, which indicated the event. The strain gages were biaxial-type gages that were installed on each of the aft hinge fittings, as shown in figure 8, to measure jettison loads transmitted to the fixed fairing and to the Centaur vehicle. Both primary and backup sets were installed identically to the proposed flight configuration. The fourth transducer configuration used was a non-flight-type piezoelectric (crystal) accelerometer. Three of these accelerometers were mounted on the spacecraft model for the first test and relocated to the spacecraft adapter for the second and third tests. They were mounted triaxially to sense the jettison shock loads transmitted to the spacecraft. Schematics of the electrical circuits and location of the transducers are shown in figure 9.

The pyrotechnic circuit battery currents were measured across a bypass shunt. Battery voltages were measured directly, but only during circuit activation to prevent voltage drain on the batteries.

Direct-indicating mechanical sensors were used to obtain two series of measurements. One type of sensor consisted of stepped lengths of soft aluminum wire probes 0.16 centimeter (1/16 in.) in diameter that were mounted on the spacecraft model at

points of critical clearance. After a test run, the longest undeflected probe in each array indicated the clearance between the fairing and the spacecraft at the associated clearance point. The other type of mechanical sensor was a spring-loaded direct-writing stylus. Sensors of this type were attached to the thermal bulkhead to measure the fore and aft maximum deflection of the bulkhead. Both types of mechanical sensors and their locations are shown in figure 10. The number and location of these sensors are given in table I.

The data from the transducers were recorded on either magnetic tape or oscillographs. The accelerometer outputs were transmitted by landline to a central data facility where the signals were recorded on frequency-modulated magnetic tape. All other transducer outputs were recorded on light beam galvanometer oscillographs located in the Space Power Facility control room.

Motion-picture cameras containing black and white film recorded specimen and equipment behavior throughout each test. Of the 15 cameras employed for the first test, 12 were located on facility mounts in the test chamber and were focused on the test fairing. The remaining three cameras were installed within the payload compartment of the fairing to record internal events. For the second and third tests, two cameras were relocated from outside the fairing to positions inside the payload compartment. All the cameras were 16-millimeter film size and were operated at 400 frames per second. The types of cameras and the specific viewing objectives are given in table I. Photographic targets were installed on the nose fairing in several locations for reference points in the films. The camera locations and the reference targets are shown in figure 11. Each camera was enclosed in a metal box having a plexiglass viewing window. The camera boxes were connected to a regulated air supply which maintained the internal pressure at approximately 4.8 newtons per square centimeter (7 psi) above the ambient pressure. This air environment prevented the "aging" effect on the film due to vacuum conditions. Also, it minimized the electrostatic discharge streaking on the film from the test chamber operating pressure.

A television camera was mounted in the test chamber and was connected to a monitor in the control room. The camera had panoramic sweep and zoom lens capabilities. This closed-circuit television system afforded a real-time view of the tests and a gross inspection of the test specimen prior to returning the test chamber to atmospheric pressure.

Calibration of the hinge load strain gages and the spacecraft shock load accelerometers was accomplished by physical methods. The strain gages were installed on the hinge fittings and calibrated on a hydraulic load fixture (fig. 12). The accelerometers were calibrated on an electromechanical shaker. All the electrical output transducer circuits were resistance calibrated immediately prior to each test and the recorder band widths were trimmed accordingly.

The jettison spring actuators were loaded and calibrated on a mechanically operated compression fixture before each test. Spring force for each actuator was as follows:

Actuator location	Test 1	Test 2	Test 3
	Spring force, N (lbf)		
Quadrant I-IV	5280 (1187)	5266 (1184)	[a]5146 (1157)
Quadrant II-III	5360 (1205)	5418 (1218)	5284 (1188)

[a]Actuator was not operated for test 3.

Subsystem Test Equipment

Of the five subsystem tests that were performed, three tests (fairing rocking, separation pull, and door open) required only minor equipment such as dial indicators, slings, and tension load dynamometers. The other two subsystem tests (radiographic clearance check and J-ring spring rate) required more extensive equipment.

The technique used to perform the radiographic checks of the spacecraft static clearance within the nose fairing employed a portable X-ray machine, a film holder, a lead reference scale, and a support fixture. The X-ray source was an Andrex 160-kilovolt machine. The film was Ansco A with 0.127-millimeter (0.005-in.) lead intensifying screen. The wooden fixture served to support and locate the X-ray equipment on the outside of the fairing. Figure 13 is a plan view of the equipment setup.

To determine the J-ring spring rate, a load fixture, a hydraulic load actuator, tension dynamometers, and a deflection measurement fixture were used. Three test arrangements were required to establish the three phases (tension, compression, and shear) of load-against-deflection characteristics. The test equipment configurations are shown in figure 14.

TEST PROCEDURE

Test Sequence

The jettison tests and the subsystem tests were intermingled to facilitate the overall schedule. The order in which the tests were performed was as follows:

(1) Static clearance check by radiography

(2) First jettison test of fairing

(3) Second jettison test of fairing

(4) Separation friction pull test
(5) Barrel section capability with access doors open
(6) Fairing twist and rocking clearance loss
(7) Third jettison test (one spring actuator inoperative)
(8) J-ring deflection test

Jettison Test Procedure

First jettison test. - For the first jettison test of the nose fairing, the test mounting assembly, consisting of the base, spacer, and simulated Centaur forward bulkhead, was installed and leveled in the center of the test chamber. On this base assembly, the major components of the test fairing and the payload assembly were erected in the following sequence:

(1) Fairing barrel section on the simulated forward tank ring
(2) J-ring on the barrel forward ring
(3) Conical adapter on the J-ring
(4) Cylindrical adapter on the conical adapter
(5) Payload adapter on the cylindrical adapter
(6) Model spacecraft on the payload adapter
(7) Fixed fairing on the J-ring
(8) Split fairing on the fixed fairing
(9) Quadrant I-IV half of nose cone on split fairing
(10) Quadrant II-III half of nose cone on split fairing

This order of assembly differed from the procedure used for the flight hardware wherein the spacecraft is encapsulated with the nose cone section in a clean-room operation and is then installed as an integral assembly. The method employed did not affect the configuration of the assembled specimen. The assembled test specimen and equipment are shown in figure 15.

After erection of the test article and prior to installation of the separation latch explosive cartridges, the pyrotechnic firing circuits were verified using fuse-type detonator simulators. The instrumentation, recorders, motion-picture cameras, photographic lighting, event timer, and event sequencer were checked for proper operation. When all test and facility systems had been confirmed through planned checks, the pyrotechnic harness assemblies were disconnected at the firing circuit relays and shorting plugs were installed as a precautionary measure. The electroexplosive cartridges were then installed in the separation latches.

An operational test of the payload compartment vent valve that was installed in the encapsulation bulkhead was performed at this point in the procedure. The system volt-

age was applied to the flapper solenoid, and a visual verification was made of the releasing mechanism in the closed position. The safety locking pin was removed and the solenoid operating circuit was deenergized. An inspection of the valve was performed to ensure that the release latch had operated, the spring-actuated flapper had swung open, and the open-position retaining latch had engaged.

After completion of the vent valve check, the shorting plugs were removed and the pyrotechnic harnesses were connected to the relay assemblies. The jettison spring actuators, which had been loaded, safety locked, and mounted in the nose cone sections prior to their erection, were unlocked by removing the safety pins. A final inspection was conducted to preclude any oversight in the total assembly, particularly in the areas of the separation planes and the jettison hardware interfaces. The service platform was secured at the base of the test specimen. Final adjustments were made to the catch nets and snubbers. The camera box purge system was activated and the closed-circuit television assembly was energized. Then the chamber hatch was secured and the remainder of the test procedure was accomplished from the control room.

Power to the control panel was switched on for equipment warmup. The pumping system was activated to evacuate the test chamber. The pumps were left operating throughout the test run. When the chamber pressure had been reduced to the equivalent of 27 432 meters (90 000 ft) altitude, the final sequence to initiate the test was performed as follows:

(1) An electrical resistance calibration was made of each transducer circuit.

(2) Photographic lighting was switched on.

(3) The magnetic tape recorder was energized.

(4) The automatic sequencer was started.

The sequencer immediately started the oscillograph recorders and the motion-picture cameras. Three seconds later it issued the command signal to the event timer which simultaneously relayed the command signal and the timing pulse to the nose fairing jettison control units and to the recorders and timing lights, respectively. Upon receipt of the command signal, the control units completed the circuits from the batteries to the detonators, thereby firing the separation latch mechanisms.

Approximately 10 seconds after the command signal, the sequencer terminated the test. A post-test electrical resistance calibration was made of the transducer circuits. The test chamber was then returned to atmospheric pressure and the access hatch opened. An inspection of the test specimen and the mechanical sensors was performed and the results recorded.

Second jettison test. - A review of the data from the first test resulted in some instrumentation changes. The accelerometers were mounted on the spacecraft adapter for more rigidity. Two motion-picture cameras were relocated from exterior positions to locations inside the fairing to record clearance probe actions. A single array of

clearance probes was located on the aft corners of each of the main panels of the spacecraft; each array was adjusted to the necessary compound angle to replace the dual arrays used on the first test. All the clearance probes were modified by addition of aluminum foil tubes on the probe ends for greater sensitivity. Battery-to-structure (ground loop) current instrumentation was added to indicate pyrotechnic detonator bridgewire shorting following cartridge firing.

In preparation for the second jettison test, the limited amount of damage sustained by the fairing and by the pyrotechnic harnesses during the first test was repaired. The jettison actuators were recalibrated and mounted in the fairing halves, and the jettisoned fairing halves (nose cone and split fairing assemblies) were reinstalled on the fixed fairing and base assembly. The procedure to complete the installation, check out the instrumentation, and initiate the second test was the same as for the first test.

Third jettison test. - For the third test, battery 2 voltage and current measurements were recorded on magnetic tape, as well as on the oscillograph, to obtain better resolution of the data. No other instrumentation changes were made.

Damage that occurred to the pyrotechnic harnesses during the second test was repaired and expendables were replaced. The fairing installation was the same as on the first two tests, except for two significant changes. The locking pin in the spring actuator of quadrant I-IV fairing half was not removed, thereby deactivating that actuator for the test; the command signal harness for the second set of pyrotechnic cartridges was not connected to the electrical system, thereby preventing activation of these cartridges. The procedure for the erection, check out, and initiation was the same as for the second test.

Subsystem Test Procedure

Fairing-spacecraft static clearance test. - Static clearance measurements between the model spacecraft solar panel hinges and the inner surface of the nose fairing were performed by X-ray photography on the fully assembled specimen. The positions opposite the spacecraft solar panel forward and aft hinges were marked on the outer skin of the fairing (fig. 13). At the location mark for hinge 1, the equipment fixture was supported against the fairing outer surface by the service elevator. The film and portable X-ray machine were mounted on the fixture. Several radiographic photographs were taken at various power adjustments and exposure times to determine the optimum conditions for the best contrast. Each of the four hinge clearances was then radiographed in sequence using the established settings. The aft hinge clearances to the fairing inner surface were also physically measured with a scale.

Separation friction pull test. - The fairing halves were remounted on the test base

following the second jettison test to perform the separation friction pull test. Latch bolts along the longitudinal split lines only were installed. Bridle harnesses with load dynamometers were connected to the fairing halves at station -40.25, as shown in figure 16. The latch bolts were removed in pairs starting at the aft end. When the last pair had been removed, the gap at the forward latch fittings (station -223.92) was measured on each side of the fairing. The fairing halves were then opened approximately 3° each to disengage the shear pins along the longerons. Maximum force values indicated on the dynamometers were recorded for starting the rotation and for holding the fairings open.

Barrel section access doors open test. - The fully assembled test specimen was used for the barrel section door open capability test. The test was limited to opening a maximum of two diametrically opposite doors (of the six access doors in the barrel section) at any time. A dial indicator for each of an opposing pair of doors was mounted independent of the specimen so that the sensing anvil was in contact with the aft ring of the fixed fairing over the center of the door opening, as in figure 17. One door of the pair was unfastened and opened. The deflection of the fixed fairing flange across the opening was sensed by the dial indicator. The second door was unfastened and opened; the deflection across both door openings was measured. The first door was closed and bolted. The deflection was measured at the open door. The second door was closed and fastened. The same procedure was used for the three pairs of opposite doors.

Fairing twist and rocking clearance loss test. - Both fairing halves were used to perform the combined twist and rocking clearance loss test. The fairings were each rotated 5° on their hinges and held open by a compression strut pinned at the forward latch fittings on the -X side, as shown in figure 18. A 444.8-newton (100-lbf) pull force normal to the jettison plane was applied in 44.5-newton (10-lbf) increments at the forward latch fitting on the -X side of the quadrant II-III fairing half. The lateral clearance was measured between the inertial boom fitting of the spacecraft and the blast shield on the +X fairing longeron for each increment of force.

J-ring deflection test. - After completion of the third jettison test, the J-ring deflection test was conducted in three phases. The jettisonable portion of the fairing was not used.

The first phase was a compression load test wherein the compression load exerted on the J-ring (fig. 14) by the model spacecraft was removed. The spacecraft was unbolted from the adapter. With a sling assembly consisting of a hydraulic lifting cylinder, spreader bar, and two dynamometers, a lifting force was applied to the spacecraft in 2224-newton (500-lbf) increments until the spacecraft was lifted clear of the assembly. Deflections of the inner edge of the J-ring and the forward ring of the cylindrical adapter were measured at the X and Y axes (fig. 14(a)).

The second phase was a tension load test. A conical fixture was fastened to the

forward end of the cylindrical adapter (fig. 14(b)). The tension load was applied in 2224-newton (500-lbf) increments to a maximum of 15 568 newtons (3500 lbf) through a sling assembly that included a hydraulic cylinder and two dynamometers. J-ring and cylindrical adapter ring deflections were measured.

The third phase was a shear load test with the force normal to the specimen centerline. The load was applied in 2224-newton (500-lbf) increments with a sling assembly (fig. 14(c)). Lateral translations and vertical deflections of the J-ring and cylindrical adapter ring were measured.

RESULTS AND DISCUSSION

Jettison Tests

In each of the three jettison tests, the fairing halves separated from each other and jettisoned clear of the forward end of the simulated vehicle and the spacecraft. All the pyrotechnic cartridges fired and all systems functioned satisfactorily. No failures occurred in any of the fairing structure or components as a result of jettison except for some latch mechanism electrical harness damage which occurred after operation because of mechanical shock loading.

The pyrotechnic firing system relay operation times, referenced to the command signal event time (T + 0 sec), are shown in figure 19. Relay 1, which connected one explosive cartridge in each of eight latches to battery 1 (fig. 7), operated at T + 0.0230 second. Relay 2, which connected one explosive cartridge in each of the other eight latches to battery 1, operated at T + 0.0237 second. Relays 3 and 4, which connect the second set of explosive cartridges (eight per relay) to battery 2, operated at T + 0.0240 and T + 0.0260 second, respectively.

In jettison test 1, battery 1 voltage and current indicated that electrical loading started at T + 0.027 second and reached a maximum of 69 amperes at T + 0.028 second, as shown in figure 20(a). This indicated relays 1 and 2 had operated and the first set of cartridges had fired. Battery 2 voltage showed loading started at T + 0.029 second. Current 2 did not increase to a maximum, however, but exhibited a negative excursion. The bridge wires of some of the second set of cartridges probably opened because of sympathetic detonation by the first set of cartridges and caused short circuits in the system after firing. The total time from operation of the earliest relay to firing of all the cartridges was 5 milliseconds, which was well within the requirement of 10 milliseconds maximum.

In jettison test 2, battery 1 current peaked at 60 amperes at T + 0.026 second, which indicated firing of the first set of cartridges. The battery 2 ground loop current

indicated shorting of the second system at the same time (fig. 20). This confirmed the belief that sympathetic firing of the second set of cartridges occurred and caused shorting of the system. The elapsed time from relay operation to cartridge firing was 3 milliseconds.

Since only the second pyrotechnic firing circuit was activated on jettison test 3 (the first circuit was disconnected), the electrical characteristics were more conclusive. The battery 2 current increased to 40 amperes at T + 0.0255 second, decreased to 5 amperes, and then increased to 50 amperes at T + 0.0275 second (fig. 20(c)). The difference in operating time between relays 3 and 4 in the circuit was 0.002 second (fig. 19). This accounted for the two distinct current peaks. First, eight cartridges were activated by relay 3 and then the other eight cartridges were activated by relay 4, which operated 2 milliseconds later. The nonactivated set 1 cartridges were detonated sympathetically by the firing of the second set. Inspection of the cartridges after the test revealed a difference in the open end of those activated electrically and those sympathetically detonated. The rolled edge of the sympathetically detonated cartridges was not expanded as in the case of the electrically activated cartridges. In tests 1 and 2, the second sets of cartridges exhibited the same effect, which confirmed that they were sympathetically fired by those set 1 cartridges that were activated first.

Some electrical harness damage of the latch cartridges was found after each test. The wire within the harness was broken at the connector. The failure of the wire was attributed to the shock of the latch nut retainer slamming against its stop after cartridge detonation. Since the damage occurred after the functional operation was completed and since only the wire and not the insulation failed so that no loose parts were generated to cause contamination, the failures did not nullify the tests.

The elapsed times from the command signal to various positions of the fairing halves during jettison as indicated by the instrumentation were as follows:

Event and fairing rotation	Quadrant I-IV fairing half			Quadrant II-III fairing half		
	Test			Test		
	1	2	3	1	2	3
	Elapsed time, sec					
Command signal	0	0	0	0	0	0
Pyrotechnic firing	0.024	0.026	0.027	0.024	0.026	0.027
Electrical bus disconnect (~13°)	0.613	0.601	0.921	0.615	0.612	0.925
Breakwire, 15° position	0.725	0.708	1.110	0.745	0.751	1.134
Breakwire, 45° position	1.677	1.693	2.351	1.695	1.689	2.334
Hinge separation (~75°)	2.16	2.15	2.85	2.21	2.21	2.90

Tests 1 and 2 showed good repeatability. Elapsed times for the events were longer on test 3, as was expected with only one of the two jettison actuators in operation (ref. 1). The angular displacements and velocities of the fairing halves with respect to time are shown in figure 21. Overall accuracies are estimated to be $\pm 2^{\circ}$ of rotation.

Figures 21(a) to (d) are plots of the rotational motions of the test fairing during the first and second jettison tests. First rotational motion of the fairing occurred within 0.035 second of pyrotechnic firing of the latch mechanisms. The delay was attributed to the inertia of the systems. As shown in the figure, the fairing motion began 0.06 second after the command signal was issued. Angular displacement of the fairing increased in a nonlinear manner during the jettison.

The angular velocity of each fairing half increased rapidly to a maximum of 31.5 degrees per second during extension of the actuators because of the energy exerted by the springs. At the end of the actuator stroke, the rotational velocity started to decrease because of the resisting force of gravity acting on the fairing halves. Earth gravity during test simulated the vehicle axial acceleration in flight at fairing jettison. However, since the input energy by the actuators greatly exceeded the energy losses of the fairing from gravity, hinge friction, and elastic body deflections, the minimum velocity was 22 degrees per second at the time the fairing center of gravity had rotated to a position vertically over the hinge. As rotation continued beyond that position, gravitational acceleration acted on the fairing to increase its angular velocity. Three events, separation of the electrical bus connectors and activation of the 15° and 45° breakwires, indicated the angular position of the fairing. These events are time oriented on the figure. Hinge separation (at the time the hinge fittings disengage) is also noted on the figure. Fairing angular motions for test 3 are indicated in figures 21(e) and (f). The displacements and velocities are similar to those of tests 2 and 3 but are smaller in magnitude because only one of the actuators was used. The fairing rotational velocity at time of actuator full extension was 18.5 degrees per second; it decreased to 13 degrees per second at the time the center of gravity was over the hinge. Although each actuator is designed to operate for 2.3° of rotation of each fairing half, energy input of one actuator less the energy losses of the fairing resulted in a positive net energy which successfully jettisoned the fairing.

Dynamic deflection of the fairing split-line longerons, which affected the clearance with the spacecraft, was a maximum at station -69 (ref. 1) where the conical and cylindrical sections interface. This was expected since the location is approximately at the midpoint between the relatively stiffer forward and aft ends of the fairing. The cyclic motion induced by the jettison force was approximately 6.7 hertz. The maximum inboard displacement toward the spacecraft was 3.3 centimeters (1.3 in.), which occurred in test 2 at the +X longeron on quadrant I-IV fairing half. At the same time, the -X longeron maximum deflection was 2.5 centimeters (1.0 in.) inboard. Test 1 maximum

inboard amplitudes were 3.0 and 2.8 centimeters (1.2 and 1.1 in.) for the +X and -X longerons of quadrant I-IV. Maximum excursions on test 3 were less than these values since only one-half of the jettison force was used. Figure 22 shows the flexing of the fairings at station -69 for the three tests. The deflection of the longerons in quadrant II-III at the time the fairing was rotating past the spacecraft inertial boom fittings (5^{o} position) determined the minimum clearance due to fairing flexure. In test 1 for that fairing position, the 2.3-centimeter (0.9-in.) inboard deflection of the -X longeron at station -69 was the largest clearance loss of the test series. Since the boom fittings are at station -40 (fig. 3), the clearance loss was corrected to 1.9 centimeters (0.75 in.). The nominal measured clearance of 10.7 centimeters (4.20 in.) less the loss from flexing of 1.9 centimeters (0.75 in.) resulted in 8.8 centimeters (3.45 in.) of clearance between the boom fitting and the -X blast shield section on the fairing longeron for the worst case. The clearances for both boom fittings in each of the three tests were as follows:

Critical clearance	Instrument number and location	Test		
		1	2	3
		Clearance, cm (in.)		
Boom fittings to quadrant II-III longeron blast shields	Instrument 28, quadrant III, -X	8.8 (3.45)	9.0 (3.53)	10.3 (4.05)
	Instrument 29, quadrant II[a], +X	8.4 (3.32)	8.0 (3.14)	9.6 (3.79)

[a]Flight configuration would not have a blast shield on +X longeron of quadrant II-III, and clearances would be 1.3 cm (0.53 in.) greater.

Accuracies are estimated to be ±0.5 centimeter (0.2 in.) based primarily on the resolution of the motion-picture film.

Clearances at critical points between the spacecraft and fairing during jettison of the test fairing were satisfactory in all cases. In test 1 the probes were not easily interpreted because of the stiffness of the aluminum wire used. Slight interference contact with the spacecraft did not yield the probe. However, the best estimate of the maximum probe lengths not contacted by the spacecraft were fairly similar, in general, to the results of test 2 wherein more sensitive probes were employed. Since the probes were arranged in incremental lengths, the clearances were at least as great as the longest undisturbed probe but not as great as the next longer probe. The ranges of clearance thus determined for the six critical locations were as follows:

Critical clearance location, fairing to spacecraft	Quadrant	Probe instrument number (fig. 9)	Test					
			1		2		3	
			Clearance range, cm (in.)					
			Min.	Max.	Min.	Max.	Min.	Max.
Encapsulation bulkhead and main solar panel aft corner	III	24	7.1 (2.8)	7.9 (3.1)	9.7 (3.8)	11.2 (4.4)	9.4 (3.7)	10.2 (4.0)
	IV	25	7.1 (2.8)	7.9 (3.1)	8.6 (3.4)	10.2 (4.0)	8.6 (3.4)	9.4 (3.7)
Encapsulation bulkhead and auxiliary solar panel aft corner	III	26	11.4 (4.5)	(a)	11.4 (4.5)	12.7 (5.0)	11.2 (4.4)	11.9 (4.7)
	IV	27	7.6 (3.6)	11.4 (4.5)	8.9 (3.5)	9.9 (3.9)	10.2 (4.0)	14.0 (5.5)
Longeron blast shield and inertial boom fitting	III	28	7.6 (3.0)	10.2 (4.0)	9.4 (3.7)	11.4 (4.5)	10.9 (4.3)	11.9 (4.7)
	II	29	7.6 (3.0)	10.2 (4.0)	8.4 (3.3)	9.7 (3.8)	10.2 (4.0)	11.9 (4.7)

[a]All probes cleared.

Four of the six clearance values at the inertial booms as determined by the flexure data were within the ranges of clearance indicated by the probes. The other two values differed by approximately the estimated accuracies. A typical probe array after test is shown in figure 23.

Thermal bulkhead deflection measurements were inconclusive on test 1 because the styli penetrated the recording pad as a result of excessive adjustment. On the other two tests, the deflection was successfully recorded. It proved to be small in the fore and aft direction and negligible in the lateral plane. The deflections at the three sensing locations were as follows:

Sensor location on quadrant II-III thermal bulkhead inner diameter	Instrument number	Test		
		1	2	3
		Fore and aft deflection, cm (in.)		
8^{o} from +X axis in quadrant II	30	(a)	±0.25 (0.10)	±0.20 (0.08)
9^{o} from -Y axis in quadrant III	31	(a)	±0.13 (0.05)	±0.13 (0.05)
8^{o} from -X axis in quadrant III	32	(a)	±0.20 (0.08)	±0.13 (0.05)

[a]Data were inconclusive.

The hinge loads as indicated by the strain gages were within the predicted ranges. Data were obtained from all the primary and backup gages on the three tests. The data from the strain gages that were arranged to sense axial loads at the hinges were directly related to the actual loads experienced, whereas the data from the strain gages sensing radial loads required correction because of the interaction of the axial load on the radial gages.

The maximum axial load on a single hinge was a compression load (applied from the forward end of the vehicle) of 8006 newtons (1800 lbf). In the radial direction, the maximum was an inboard load (applied inward toward the center of the vehicle) of 2268 newtons (510 lbf). The maximum total axial force exerted at one time by a fairing half on its pair of hinges was 12 680 newtons (2850 lbf) of compression load by quadrant I-IV. At that time, the total radial load was 2180 newtons (490 lbf) of outboard force. The maximum total radial load by a fairing half was 3510 newtons (790 lbf) of outboard force with a total axial compression load of 7390 newtons (1660 lbf) at the same time. Other load data are shown in table II.

Complex dynamic load vibrations were evident during the early part of the jettison on each test. In general, there was a 1000-hertz vibration at the beginning of all hinge traces on all tests for the first 0.1 to 0.2 second. This was followed by the appearance of a 400-hertz vibration of slightly larger amplitude, which developed into a 200-hertz vibration. Fairing large load cycles of 25 to 30 hertz axial and 7 to 8 hertz radial appeared on almost all hinge traces. On the fairing halves there was a 2-hertz rocking in most cases.

Additional results obtained from the hinge strain gage data categorized by test and fairing half were as follows:

Test 1. - The additional results for test 1 are as follows:

Quadrant I-IV - axial loads: Hinge 1 showed a rapid load pickup starting at T + 0.04 second, while hinge 2 showed a slow load buildup starting at T + 0.05 second. Some 25-hertz vibration was noticeable in both hinges, in phase, from T + 0.12 to T + 0.40 second. Rocking began from the first indication of load and continued until T + 2.00 second, when it became difficult to detect.

Quadrant I-IV - radial loads: In addition to the 25-hertz signal variations caused by the axial load vibrations, there was an out-of-phase vibration in the two hinges at about 8 hertz until T + 1.20 seconds. Hinge 1 had flat periods of zero radial load at T + 0.13, T + 0.17, T + 0.21, and T + 0.47 second. Hinge 1 had large load variations in the period from T + 0.65 to T + 1.00 second (1469 N or 330 lbf outboard to 890 N or 200 lbf inboard). Hinge 2 had similar variations from T + 0.9 to T + 1.33 seconds. Beyond these times, the loads were relatively free of vibration.

Quadrant II-III - axial loads: Hinges 3 and 4 load pickup was simultaneous with about the same peak loads. Almost no rocking was detectable. A large amplitude vi-

bration, in phase on both hinges, at about 25 hertz continued until T + 1.30 seconds.

Quadrant II-III - radial load: There was a large amplitude vibration, in phase on both hinges, of about 8 hertz which started T + 0.10 second and continued until disengagement.

Test 2. - The additional results of test 2 were as follows:

Quadrant I-IV - axial loads: Hinge 1 had a large load cycle to about T + 0.10 second before hinge 2 showed much load. From then to about T + 0.60 second, the two hinge vibrations were in phase but the frequency varied. The predominant frequency was about 30 hertz. After T + 0.60 second, the two hinges were out of phase. From T + 0.63 to T + 0.83 second, hinge 2 showed almost no load, while hinge 1 carried the fairing load. At T + 0.83 second, the load began to shift from hinge 1 to hinge 2, which carried the load alone until T + 1.20 seconds. At T + 1.56 seconds, the load shifted back to hinge 1. By T + 2.00 seconds, there was essentially no load in the axial direction on either hinge.

Quadrant I-IV - radial loads: There was a predominat 7.5-hertz oscillation of both hinges 1 and 2 from T + 0.15 to T + 0.90 second. After T + 0.90 second, hinge 1 radial loads damped down to small oscillations of less than 890 newtons (200 lbf) and low frequency. After T + 0.90 second, hinge 2 continued to experience 7.5-hertz frequency until T + 1.90 seconds.

Quadrant II-III - axial loads: The quadrant II-III fairing half exerted a load on both hinges simultaneously with approximately equal load on each hinge. Both hinges showed a varying frequency, in phase, with a predominant frequency of about 25 to 30 hertz from T + 0.17 to T + 0.7 second. From T + 0.7 second to separation, there was some evidence of rocking at a frequency of about 3 hertz, but loads were generally constant with the greater load on hinge 3. There was no evidence of "lift-off" of either hinge throughout the entire rotation. Disengagement was clearly shown at T + 2.20 seconds for both hinges.

Quadrant II-III - radial loads: Both radial loads were comparatively small until T + 0.16 second. During this time, both hinges showed two small outboard excursions. The two hinges showed an in-phase oscillation of about 7 hertz throughout the entire rotation. As shown in table II, some significant outboard loads occurred on both hinges.

Test 3. - The additional results for test 3 are as follows:

Quadrant I-IV - axial loads: Hinge 1 showed buildup of significant load to T + 0.07 second, when hinge 2 showed the beginning of load buildup. Starting at T + 0.11 second, the two hinges are in phase at about 30 hertz with load varying ±445 newtons (100 lbf). At T + 0.53 second, a pronounced rocking became evident at about 2 hertz with the hinges going alternately to zero axial load for three cycles. This was similar to test 2. At T + 2.10 seconds, the rocking damped out and the axial loads were relatively con-

stant until disengagement at T + 2.80 seconds for hinge 2 and T + 2.85 seconds for hinge 1.

Quadrant I-IV - radial loads: There was a predominant load oscillation of both hinges 1 and 2 of about 7.5 hertz, in phase, to about T + 0.95 second. From T + 0.95 to T + 1.25 seconds, hinge 1 showed a steady load, while hinge 2 was oscillating at about ±445 newtons (100 lbf). At T + 1.25 seconds, hinge 1 started oscillating, and hinge 2 was relatively steady until T + 1.55 seconds. From that time until disengagement, both hinge loads oscillated slightly out of phase at about 7.5 hertz.

Quadrant II-III - axial loads: The quadrant II-III fairing half had unusual data. Rocking action at 2.5 hertz clearly began at T + 0.37 second and continued until T + 2.20 seconds, when it became less obvious. From T + 0.40 to 0.64 second, hinge 4 showed zero load, while hinge 3 carried all the load with oscillations of 25 hertz superimposed. Both hinges picked up load, with the load on hinge 4 going a little higher and then dropping to zero. Small high-frequency vibrations were present and the hinges were in phase at 25 hertz from T + 0.10 to T + 0.40 second.

Quadrant II-III - radial loads: Both hinges showed little vibration except for a small amount of high-frequency vibration during the first 0.10 second. Hinge 4 showed a period of zero load from T + 0.40 to 0.64 second, corresponding to the axial trace. No phase relation was shown because of the lack of load vibration. Both hinges showed a variation in radial load which was in phase with the rocking of the fairing.

The shock loads transmitted to the spacecraft inertial model were of acceptable magnitude and duration. On the first test, although the calibrated ranges of the accelerometers were exceeded, the estimated magnitudes of the loads were considered to be less than the shock level the spacecraft would experience in flight from the payload separation pyrotechnics. These explosive cartridges are located immediately adjacent to the aft end of the spacecraft with a direct transmission path for the shock load, whereas the nose fairing pyrotechnic firing shock must be transmitted aft through the fairing to the payload adapter and then forward through the adapter to the spacecraft, thereby damping the force.

The accelerometers for test 1 were mounted on the spacecraft structure. For tests 2 and 3 they were mounted on the spacecraft adapter, which was a much more rigid structure. As a result, the shock loads recorded during test 1 were higher than those recorded during tests 2 and 3. The initial and maximum shock loads and the frequencies generated were as follows:

Direction of sensitivity of accelerometer (vehicle axes)	Test								
	1			2			3		
	Shock load (zero to peak)								
	g's		Frequency, Hz	g's		Frequency, Hz	g's		Frequency, Hz
	Initial	Maximum[a]		Initial	Maximum		Initial	Maximum	
Longitudinal axis (Z-Z)	67	110	650	38	55	1000	35	70	1150
Perpendicular to split line (Y-Y)	65	105	750	20	52	1000	20	52	750
Parallel to split line (X-X)	60	130	550	12	53	1000	10	40	750

[a]Maximum loads for test 1 were beyond calibrated range of accelerometers and are estimated values.

The shock loads decayed to 50 percent of maximum value in 40 milliseconds for test 1 and in 15 milliseconds for tests 2 and 3.

Subsystem Tests

Fairing-spacecraft static clearance test. - Measurement of the static clearance between the spacecraft solar panel hinges and the inside of the nose fairing by radiographic technique was very successful. Good density differential was attained on the film for the aluminum alloy hinges and the fiber-glass honeycomb core. The optimum setting for the 160-kilovolt portable X-ray machine was 110 kilovolts, 4.5 milliamperes for 4 minutes duration. Clearances determined from the photographs of the four critical clearance points and the measured clearances for the aft two points (the forward two points were inaccessible for physical measurement) were as follows:

Hinge number (ref. 12)	Clearance, cm (in.)	
	By radiography	By measurement
1	7.85 (3.09)	7.85 (3.09)
2	7.96 (3.13)	7.94 (3.12)
3	7.35 (2.89)	----------
4	6.76 (2.66)	----------

Separation friction pull test. - The force required to overcome the static friction in starting the fairing rotation was small. Approximately 89 newtons (20 lbf) was required on each fairing half. At the start of the test when the latch bolts were removed, the fairing gapped slightly because of the compressive force in the split-line seal. The gap was 0.97 centimeter (0.38 in.) at the -X longeron forward latch fitting and 0.76 centimeter (0.30 in.) on the +X side. The force required to start rotation was 556 newtons (125 lbf) per fairing half, and 467 newtons (105 lbf) was required to hold the fairing open at approximately 3^{o}. Since the fairing halves had a maximum mismatch at installation along the -X longeron of 1.0 centimeter (0.4 in.) at station -69, the static friction was composed of hinge friction and split-line shear pin friction from the lateral mismatch force.

Barrel section access doors open test. - The maximum deflection on the aft flange of the fixed fairing section with one access door open in the barrel section was 0.11 centimeter (0.042 in.). This maximum deflection occurred at door 6 (fig. 17). With the diametrically opposite door 3 open simultaneously, no increase in deflection was indicated. The deflection at door 3 was 0.02 centimeter (0.006 in.). The other two pairs of doors caused 0.03 and 0.02 centimeter (0.011 and 0.009 in.) of deflection at doors 4 and 1, respectively, and 0.04 and 0.01 centimeter (0.017 and 0.004 in.) at doors 2 and 5, respectively. Each access door was opened and closed without experiencing any binding, except for door 6 which scraped slightly during closing.

Fairing twist and rocking clearance loss test. - The lateral force normal to the jettison plane, which was applied to the quadrant II-III fairing half, rocked the fairing on its pair of hinges until all the hinge clearance was removed and the fairing was tipped laterally to the extreme rigid-body position. Simultaneously, the force twisted the fairing half about the shear center, causing elastic torsional deflection. The clearance loss between the spacecraft inertial boom fittings and the nose fairing longeron for the combined rigid-body and elastic torsional deflections is shown in figure 24.

The equivalent force applied at the forward latch to produce a rigid-body moment equal to the expected maximum yaw acceleration of 0.05 g acting on the fairing center of gravity in flight at nose fairing jettison is 126.8 newtons (28.5 lbf). The moment caused by this force is not sufficient to overcome the moment caused by the fairing weight, and there will be no clearance loss from rigid-body deflection in flight. However, the torque about the fairing shear center equivalent to the torque that would be produced by the maximum expected yaw at jettison is 170.4 newtons (38.3 lbf) applied at the forward latch. For this force, the maximum clearance loss from torsional deflection would be 0.76 centimeter (0.3 in.) during fairing jettison in flight.

J-ring deflection test. - The axial deflections measured at the inner edge of the J-ring were small when the spacecraft compressive load of 18 895 newtons (4248 lbf) was removed from the specimen. Deflections ranged from 0.0025 to 0.0178 centimeter

(0.001 to 0.007 in.) at the four locations that were sensed (fig. 14). For the largest deflection, this was equivalent to a spring rate of 1050 kilonewtons per centimeter (600 000 lbf/in.). The maximum deflection produced by the tension load of 15 724 newtons (3535 lbf) that was applied to the J-ring was 0.0102 centimeter (0.004 in.). This was equivalent tc 1540 kilonewtons per centimeter (880 000 lbf/in.). The results of the shear load test on the J-ring were inconclusive, as the base structure supporting the test specimen deflected and allowed the measuring indicators to develop relative motion.

Comparison with Flight Data

The first flight of an Orbiting Astronomical Observatory spacecraft (OAO-A2) on an Atlas-Centaur launch vehicle employed several nose fairing instruments that were identical in model and arrangement to those used in the jettison test. A good comparison of the flight and test data, therefore, was readily accomplished (ref. 2).

The X-ray photography technique that was developed during the test program to verify the spacecraft-fairing static clearance (axial alinement) was used on the flight article. The radiographs of the four checkpoints were well defined and indicated that the static clearance was 6.9 centimeters (2.7 in.) at the closest point. This was above the minimum allowable clearance of 6.4 centimeters (2.5 in.).

OAO-A2 launch vehicle elapsed times from the latch pyrotechnic cartridge firing to the 15^{o} position, to the 45^{o} position, and to hinge separation compared well with tests 1 and 2 data. This indicated that both spring thrusters operated and that the flight fairing jettisoned successfully. The elapsed times for the flight and test events are as follows:

Event and fairing rotation angle	Quadrant I-IV fairing				Quadrant II-III fairing			
	OAO-A2 flight[a]	Test[b]			OAO-A2 flight[a]	Test[b]		
		1	2	3		1	2	3
	Elapsed time, sec							
Pyrotechnic firing	0	0	0	0	0	0	0	0
15^{o} Breakwire position	0.673	0.701	0.682	1.083	0.639	0.721	0.725	1.107
45^{o} Breakwire position	1.645	1.653	1.667	2.324	1.644	1.671	1.663	2.307
Hinge separation	2.14	2.14	2.13	2.82	2.24	2.19	2.18	2.87

[a] 0.8-g acceleration at nose fairing jettison.

[b] 1-g gravity field during test.

Also, the hinge loads experienced on OAO-A2 flight compared favorably with those recorded on the tests. The maximum loads on the hinges during jettison for the flight and tests were as follows:

Type of load	OAO-A2 flight[a]				Jettison test individual hinge[b]		OAO-A2 flight[a]		Jettison test fairing half combined hinges[b]	
	Hinge 1	Hinge 2	Hinge 3	Hinge 4	Test 1	Test 2	+Y fairing half combined hinges 1 and 2	-Y fairing half combined hinges 3 and 4	Test 1	Test 2
	Load, N (lbf)									
Maximum axial compression	4670 (1050)	6894 (1550)	4893 (1100)	9341 (2100)	8006 (1800)	7117 (1600)	10 898 (2 450)	9118 (2050)	12 677 (2 850)	11 565 (2 600)
Maximum axial tension	None	None	445 (100)	None	None	None	None	None	None	None
Maximum radial acting inboard	1801 (405)	1312 (295)	2513 (565)	1023 (230)	1913 (430)	2268 (510)	1 957 (440)	3269 (735)	2 980 (670)	3 247 (730)
Maximum radial acting outboard	1557 (350)	2068 (465)	1913 (430)	2291 (515)	1913 (430)	2180 (490)	2 669 (600)	2291 (515)	3 158 (710)	3 514 (790)

[a] 0.8-g acceleration at nose fairing jettison.
[b] 1-g gravity field during test.

CONCLUSIONS

The Centaur-OAO nose fairing altitude jettison test results show that the separation system is capable of satisfactorily jettisoning the bisegmented fairing at altitude and that the fairing has structural capability to withstand the jettison forces. Further, the fairing halves will separate and jettison with one of the dual sets of pyrotechnic firing circuits activated and with one of the two spring thrusters operative.

Predicted fairing trajectories, with jettison produced by one or both spring thrusters, is satisfactory. The clearances between the spacecraft and the fairing during jettison, including losses from dynamic deflections, is adequate for worst-case conditions.

Deflection of the thermal bulkhead is insignificant and presents no clearance problem with the equipment mounted on the forward bulkhead of the vehicle. Tests showed that the hinge loads are well within the acceptable levels. Shock loads to the spacecraft from the detonation of the pyrotechnic cartridges in the fairing separation latches are not excessive.

Subsystem tests showed that the barrel section (on which the fairing, the payload adapters, and the spacecraft are mounted) is capable of supporting the static load during ground servicing with any two diametrically opposite access doors open. Tests were not performed to ascertain if more than two doors can be opened at one time, as service requirements can be fulfilled by access through two doors. Clearance loss from maximum predicted yawing of the vehicle at fairing jettison combined with losses from fair-

ing flexure is not expected to diminish the clearance at the inertial boom fitting on the spacecraft sufficiently to violate the desired clearance margin. The J-ring has a large spring rate and, therefore, only small deflections will result from the inertial loads imposed by the spacecraft.

It was determined that the static clearance between the spacecraft and the inner surface of the fairing (the axial alinement) can be measured accurately by radiographic technique following erection of the encapsulated payload on the vehicle at the launch site. In addition, the subsystem tests showed that the design criterion for the mismatch of the fairing halves was sufficiently limiting to prevent significant friction losses during separation of the fairing.

The capability of the nose fairing separation and jettison system to function satisfactorily at altitude was further verified by OAO-A2 flight results.

Lewis Research Center,
National Aeronautics and Space Administration,
Cleveland, Ohio, June 5, 1970,
491-01.

REFERENCES

1. Anon.: Engineering Study to Support Centaur OAO-A2 Mission. Vol. I. Rep. GDC BTD67-043-3, General Dynamics Corp., 1967.
2. Staff of Lewis Research Center: Atlas-Centaur AC-16 Flight Performance Evaluation for the Orbiting Astronomical Observatory OAO-II Mission. NASA TM X-1989, 1970.

TABLE I. - SUMMARY OF INSTRUMENTATION, DATA RECORDERS, AND CAMERAS

[All cameras of 16-mm film size and operated at 400 frames per sec.]

(a) Instruments and data recorders

Instrument			Parameter measured	Range of instrument	Data recorder
Number	Type	Location			
1	Breakwire	Quadrant II-III	15^{o} rotation position	On-off	Light beam galvanometer oscillograph
2		Quadrant II-III	45^{o} rotation position		
3	Bus disconnect	Quadrant II-III	Harness separation		
4	Breakwire	Quadrant I-IV	15^{o} rotation position		
5		Quadrant I-IV	45^{o} rotation position		
6	Bus disconnect	Quadrant I-IV	Harness separation		
7	Strain gage	Hinge 1	Axial load	17 800 N (4000 lbf) compression to 4450 N (1000 lbf) tension	
8		Hinge 2			
9		Hinge 3			
10		Hinge 4			
11		Hinge 1	Radial load	8900 N (2000 lbf) inboard to 2225 N (500 lbf) outboard	
12		Hinge 2			
13		Hinge 3			
14		Hinge 4			
15	Direct	Battery 1	Pyrotechnic firing voltage	0 to 45 V	
16		Battery 2			

17	Shunt	Battery 1	Pyrotechnic firing current	0 to 200 A	
18		Battery 2			
[a]19		Battery 1	Ground loop current	0 to 100 A	
[a]20		Battery 2			
21	Accelerometer	Spacecraft[b]	Shock load, vehicle X axis	0 to 100 g's	FM magnetic tape
22			Shock load, vehicle Y axis	0 to 100 g's	
23			Shock load, vehicle Z axis	0 to 75 g's	
24	Sensor probe	Solar panel aft corner, quadrant III	Clearance to fairing encapsulation bulkhead	2.5 to 15.2 cm (1 to 6 in.)	Direct deflection
25		Solar panel aft corner, quadrant IV			
26		Auxiliary panel, quadrant III	Clearance to fairing encapsulation bulkhead	5.0 to 14.0 cm (2 to 5.5 in.)	
27		Auxiliary panel, quadrant IV			
28		Inertial boom fitting, quadrant III	Clearance to fairing longerons	2.5 to 12.7 cm (1 to 5 in.)	
29		Inertial boom fitting, quadrant II			
30	Stylus	+X axis	Thermal bulkhead deflection	2.5 cm (1 in.)	Direct write-out
31		-Y axis			
32		-X axis			

[a]Not installed for test 1.

[b]Located on aft end of spacecraft for test 1 and on spacecraft adapter for tests 2 and 3.

TABLE I. - Concluded. SUMMARY OF INSTRUMENTATION, DATA RECORDERS, AND CAMERAS

[All cameras of 16-mm film size and operated at 400 frames per sec.]

(b) Motion-picture cameras

Camera	Lens focal length, mm	Viewing target	Parameter	Camera location relative to test specimen	Camera used in tests-
1	10	Quadrant I-IV fairing	Initial trajectory	External	1, 2, 3
1A		Quadrant I-IV fairing	Terminal trajectory		
2		Quadrant II-III fairing	Initial trajectory		
2A		Quadrant II-III fairing	Terminal trajectory		
3		Quadrant I-IV fairing	Lateral motion		
4		Quadrant II-III fairing			
5	25	Quadrant I-IV hinge 2	Hinge operation		
6		Quadrant II-III hinge 3			
7	10	Nose cap area	Separation latch and spring actuator operation		1
		Solar panel corner, quadrant III	Encapsulation bulkhead head clearance	Internal	2, 3
8		Quadrant I-IV electrical harness disconnects	Disconnect operation		1, 2, 3
9		Quadrant II-III electrical harness disconnects			
10		Encapsulation bulkhead seal release and vent valve, quadrant II	Seal release and valve latch operation		
11	25	Mechanical interlock, +X axis	Interlock operation	External	1
		Solar panel corner, quadrant IV	Encapsulation bulkhead clearance	Internal	2, 3
12		+X split line	+X longeron flexing	External	1, 2, 3
13		-X split line	-X longeron flexing		

[a]Not installed for test 1.

[b]Located on aft end of spacecraft for test 1 and on spacecraft adapter for tests 2 and 3.

TABLE II. - NOSE FAIRING MAXIMUM HINGE LOADS

[Time is from pyrotechnic firing command.]

(a) Individual hinge loads

Load condition			Test 1				Test 2				Test 3			
			Hinge				Hinge				Hinge			
			1	2	3	4	1	2	3	4	1	2	3	4
Axial compression[a]		Load, N (lbf)	6405 (1440)	8006 (1800)	4670 (1050)	6316 (1420)	6227 (1400)	7117 (1600)	5338 (1200)	6227 (1400)	5338 (1200)	4982 (1120)	6138 (1380)	5427 (1220)
		Time, sec	0.72	0.16	0.45	0.19	0.72	0.14	0.18	0.18	0.66	0.16	0.58	0.80
Radial	Inboard	Load, N (lbf)	890 (200)	934 (210)	1557 (350)	1913 (430)	1334 (300)	2268 (510)	1557 (350)	1690 (380)	890 (200)	801 (180)	890 (200)	1334 (300)
		Time, sec	0.35	0.98	0.52	0.25	0.36	0.14	0.24	0.24	0.86	2.41	1.86	2.28
	Outboard	Load, N (lbf)	1468 (330)	1913 (430)	1379 (310)	1779 (400)	2046 (460)	2180 (490)	1690 (380)	1824 (410)	1201 (270)	1957 (440)	1112 (250)	1023 (230)
		Time, sec	0.69	0.44	0.58	0.58	0.56	0.42	0.58	0.58	0.66	0.41	1.21	0.95

(b) Fairing half combined hinge loads

Load condition			Test 1		Test 2		Test 3	
			Fairing half		Fairing half		Fairing half	
			Quadrant I - IV	Quadrant II - III	Quadrant I - IV	Quadrant II - III	Quadrant I - IV	Quadrant II - III
Axial compression[a]		Load, N (lbf)	12 677 (2 850)	10 764 (2 420)	10 675 (2 400)	11 565 (2 600)	6672 (1500)	8273 (1860)
		Time, sec	0.16	0.19	0.14	0.18	0.16	0.16
Radial	Inboard	Load, N (lbf)	756 (170)	2 980 (670)	1 423 (320)	3 247 (730)	756 (170)	978 (220)
		Time, sec	0.49	0.25	0.14	0.25	2.41	2.28
	Outboard	Load, N (lbf)	2 357 (530)	3 158 (710)	3 158 (710)	3 514 (790)	2446 (550)	1156 (260)
		Time, sec	0.44	0.58	0.42	0.58	0.41	1.11

[a]Axial tension loads were not evident, only axial compressive loads were experienced.

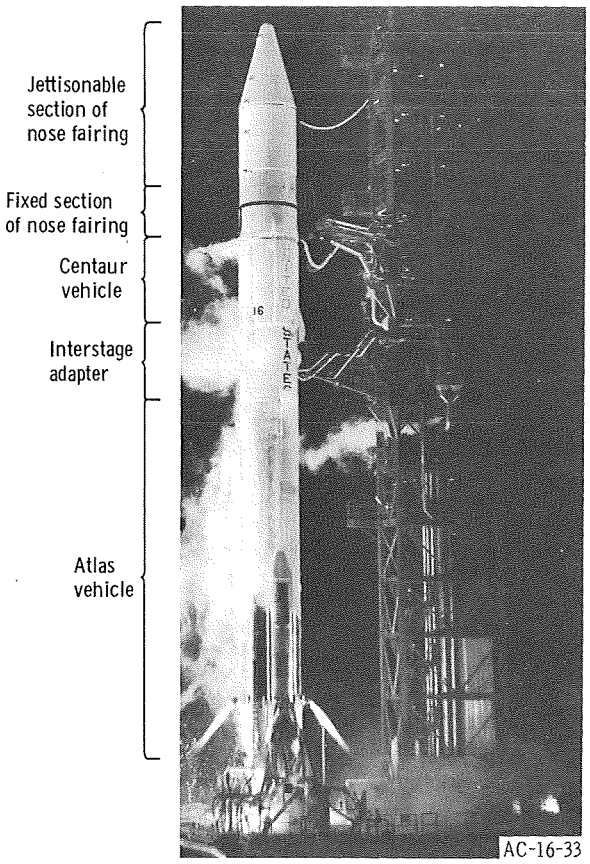

Figure 1. - Atlas-Centaur launch vehicle with OAO nose fairing.

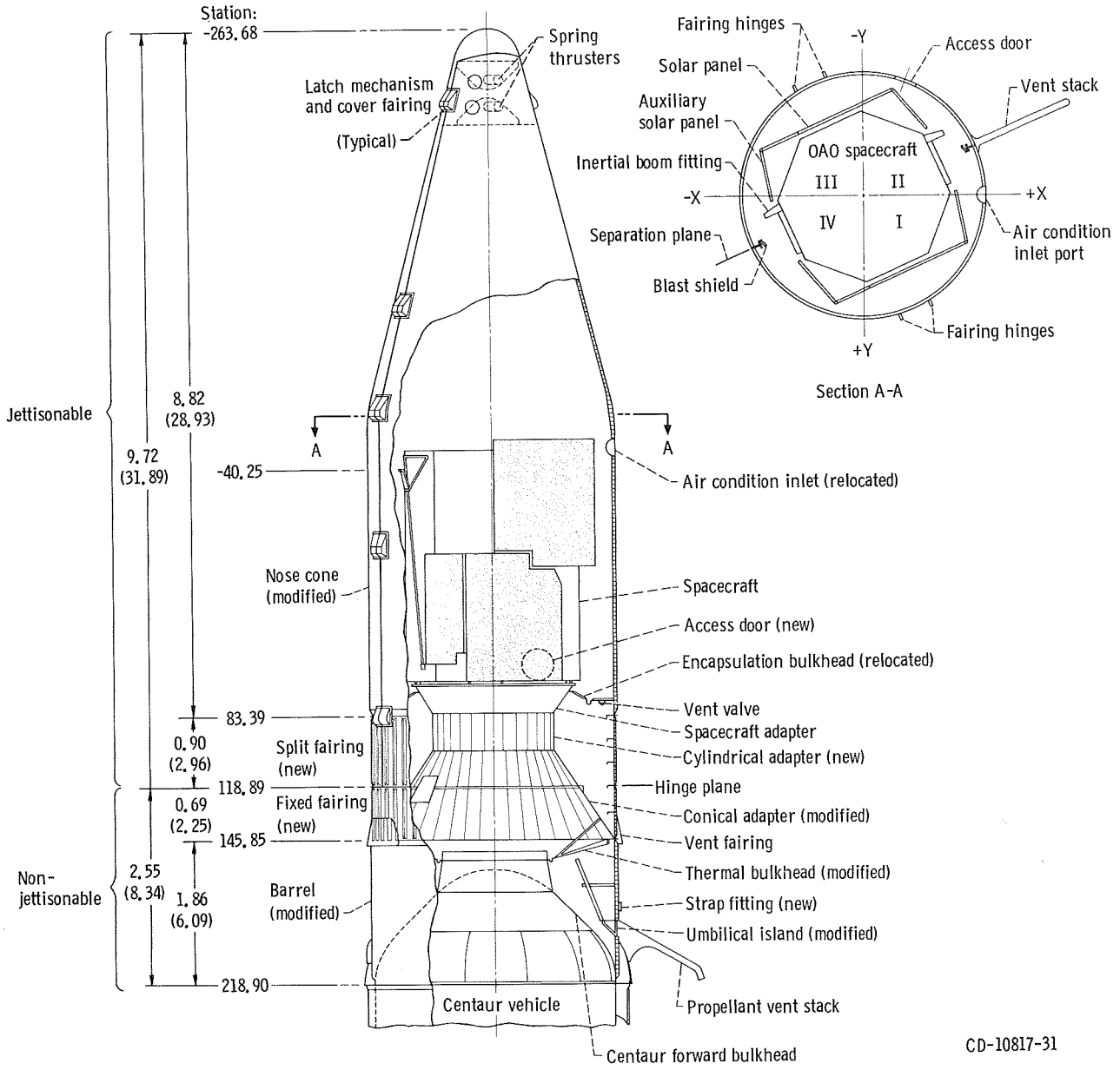

Figure 2. - Centaur-OAO nose fairing and payload adapter configuration. (All dimensions are in meters (ft).)

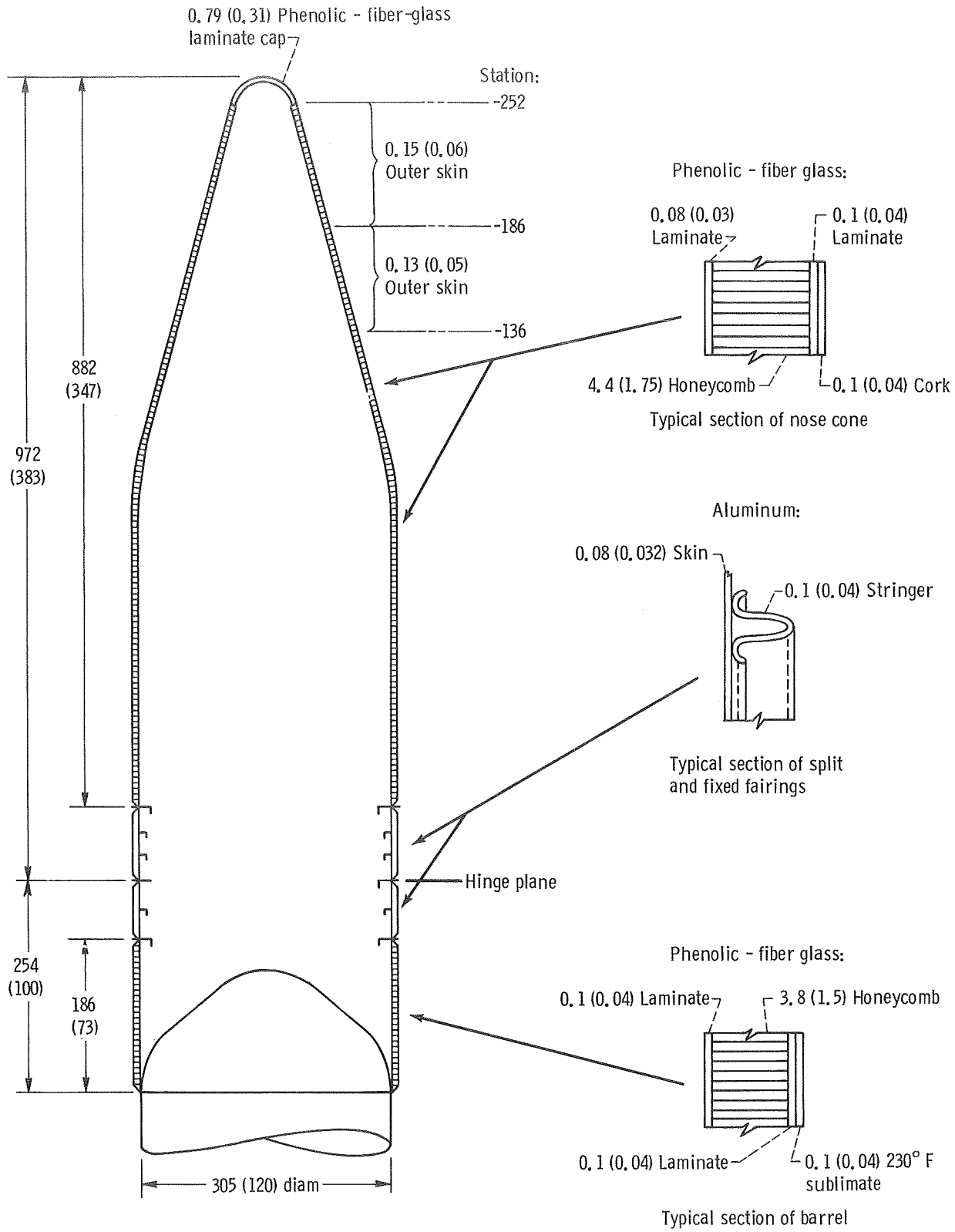

Figure 3. - Centaur-OAO nose fairing dimensions. (All dimensions are in centimeters (in.).)

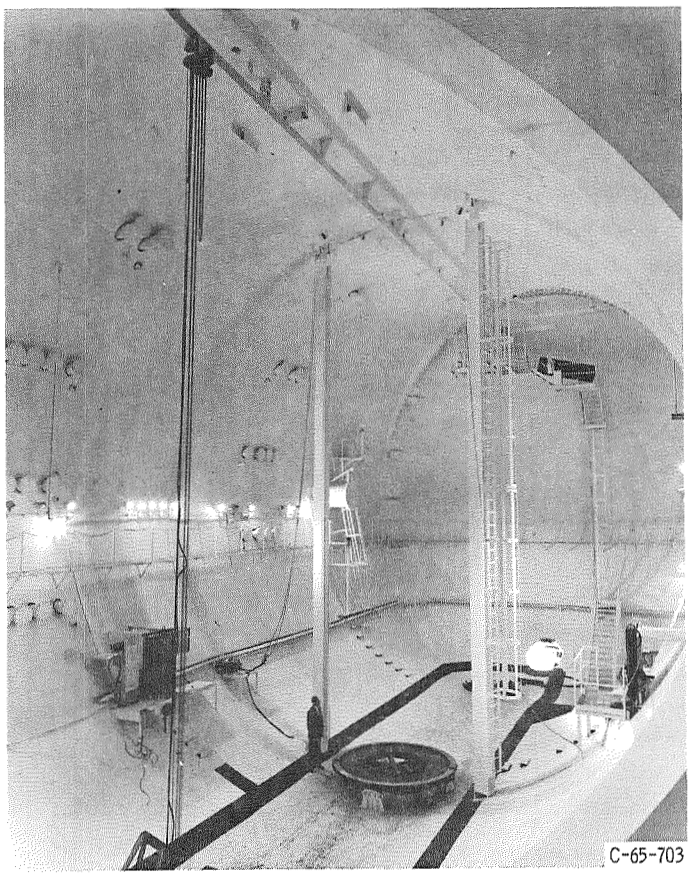

Figure 4. - Test chamber 2, Space Power Chamber Facility.

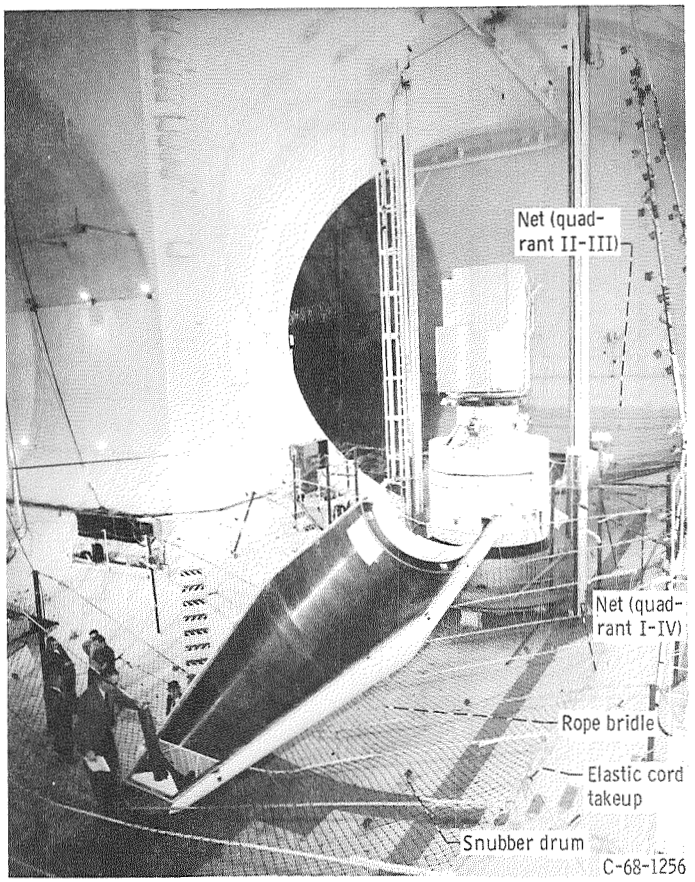

Figure 5. - Catch net and anti-rebound system.

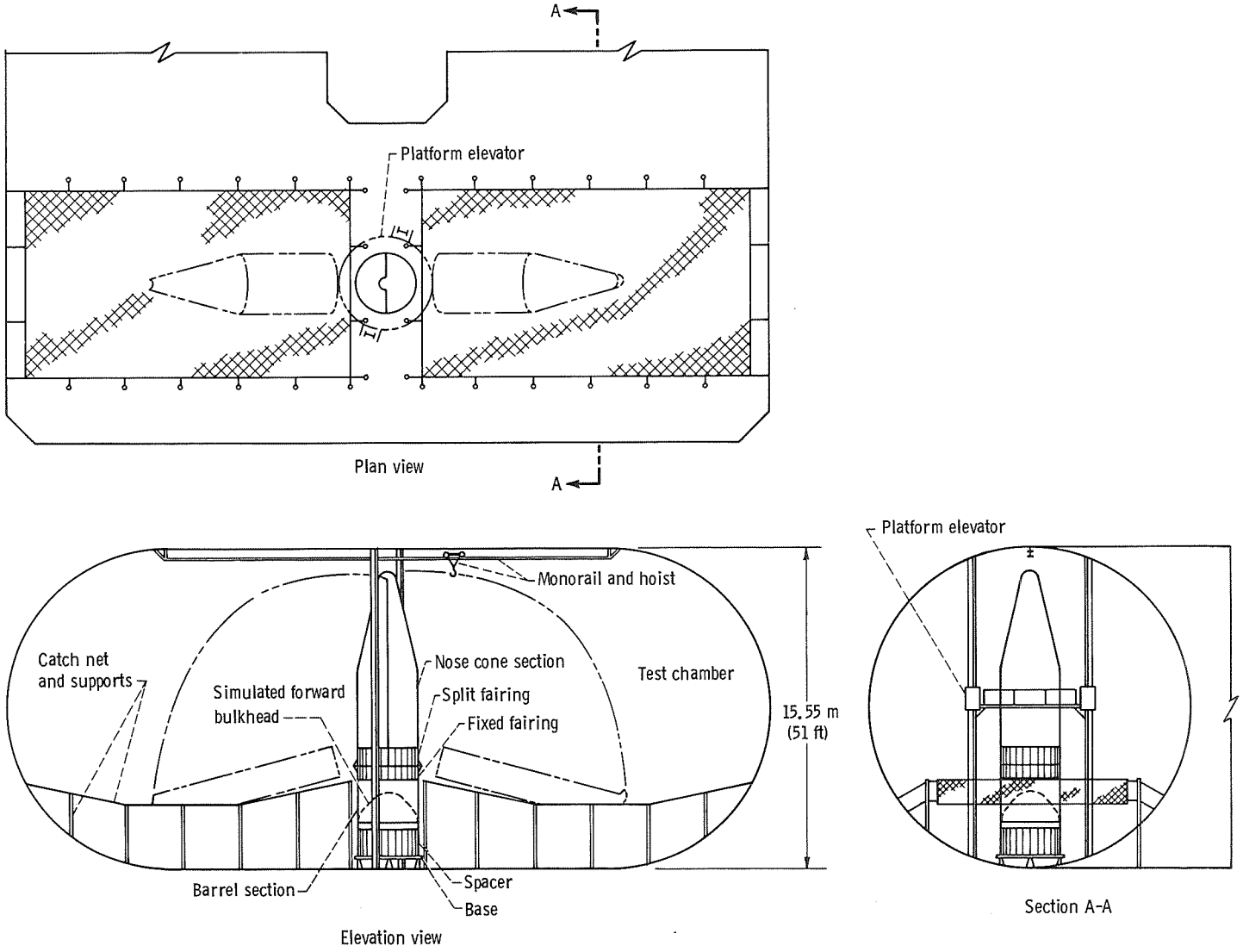

Figure 6. - Test equipment and test specimen arrangement in test chamber.

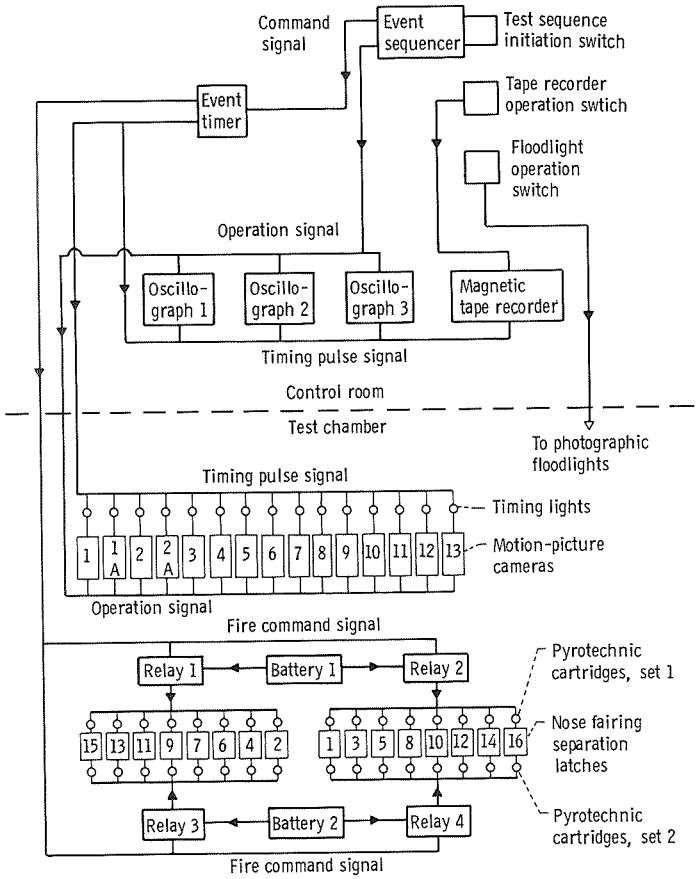

Figure 7. - Jettison test control system.

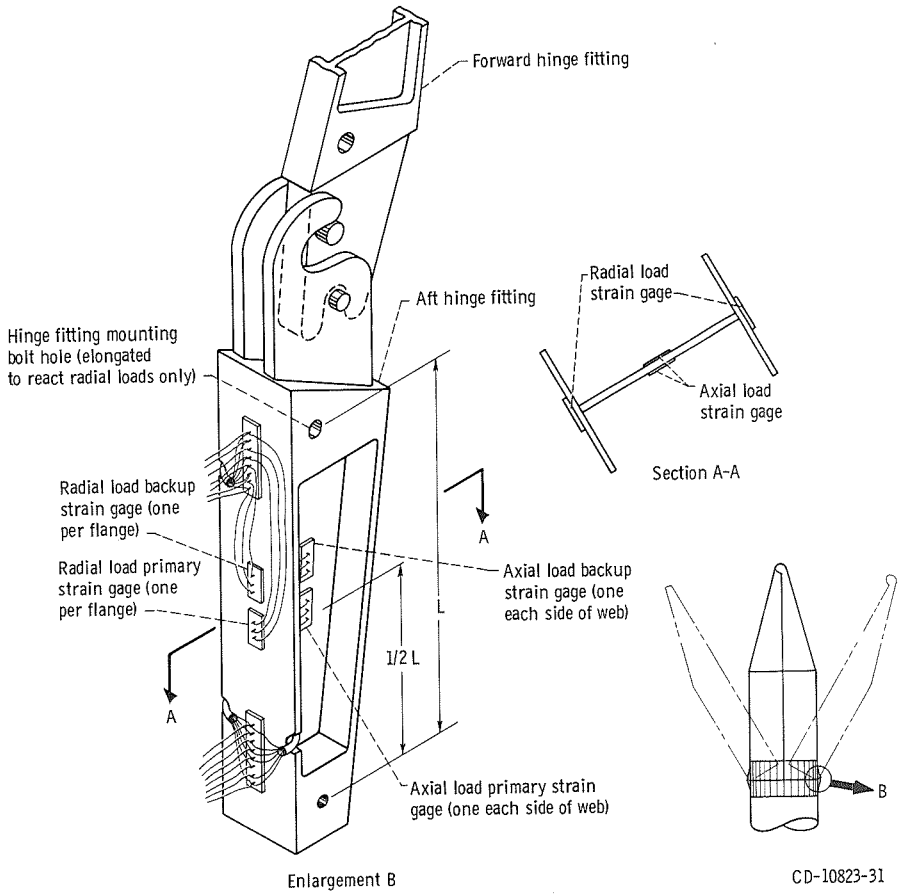

Figure 8. - Typical strain gage installation on hinge fitting. (All strain gages are biaxial for temperature compensation and augmented output.)

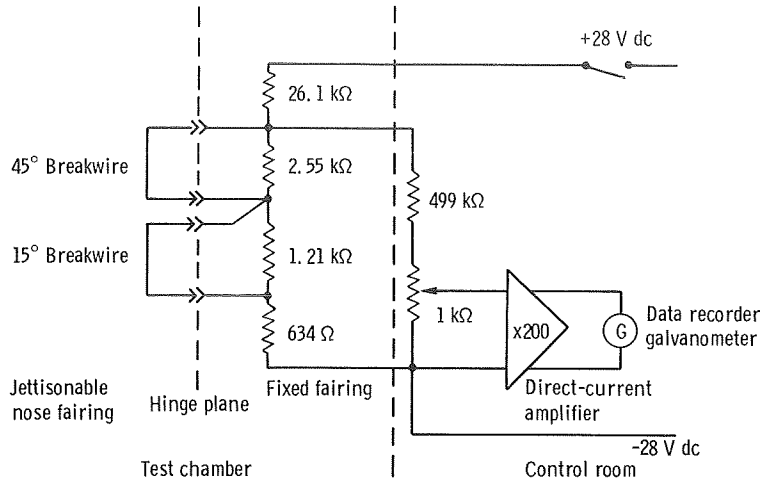

(a) Typical angular motion breakwire schematic.

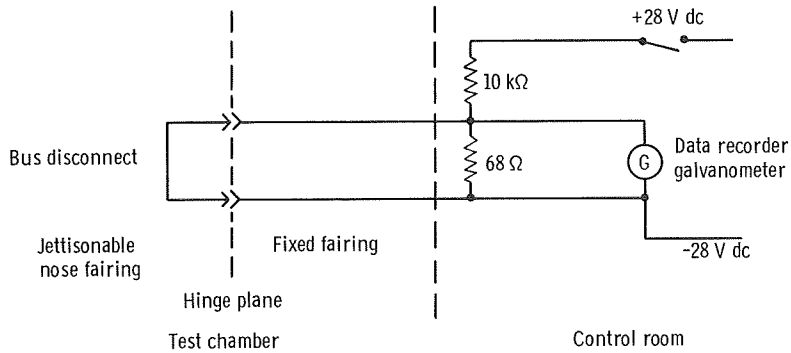

(b) Typical electrical bus disconnect schematic.

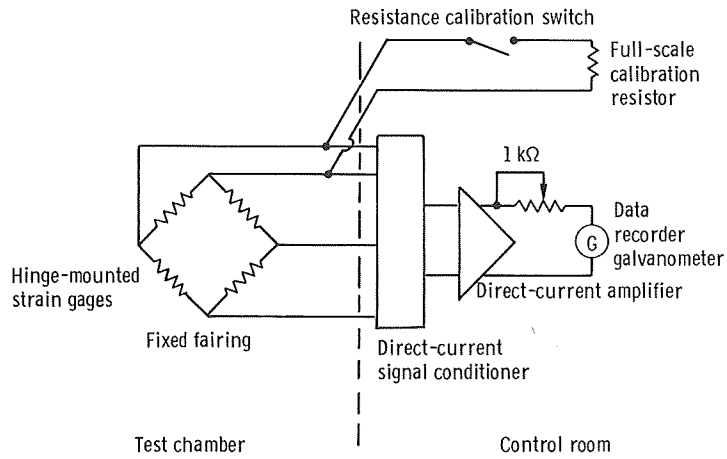

(c) Typical hinge strain gage schematic.

Figure 9. - Instrumentation electrical transducer schematics and locations.

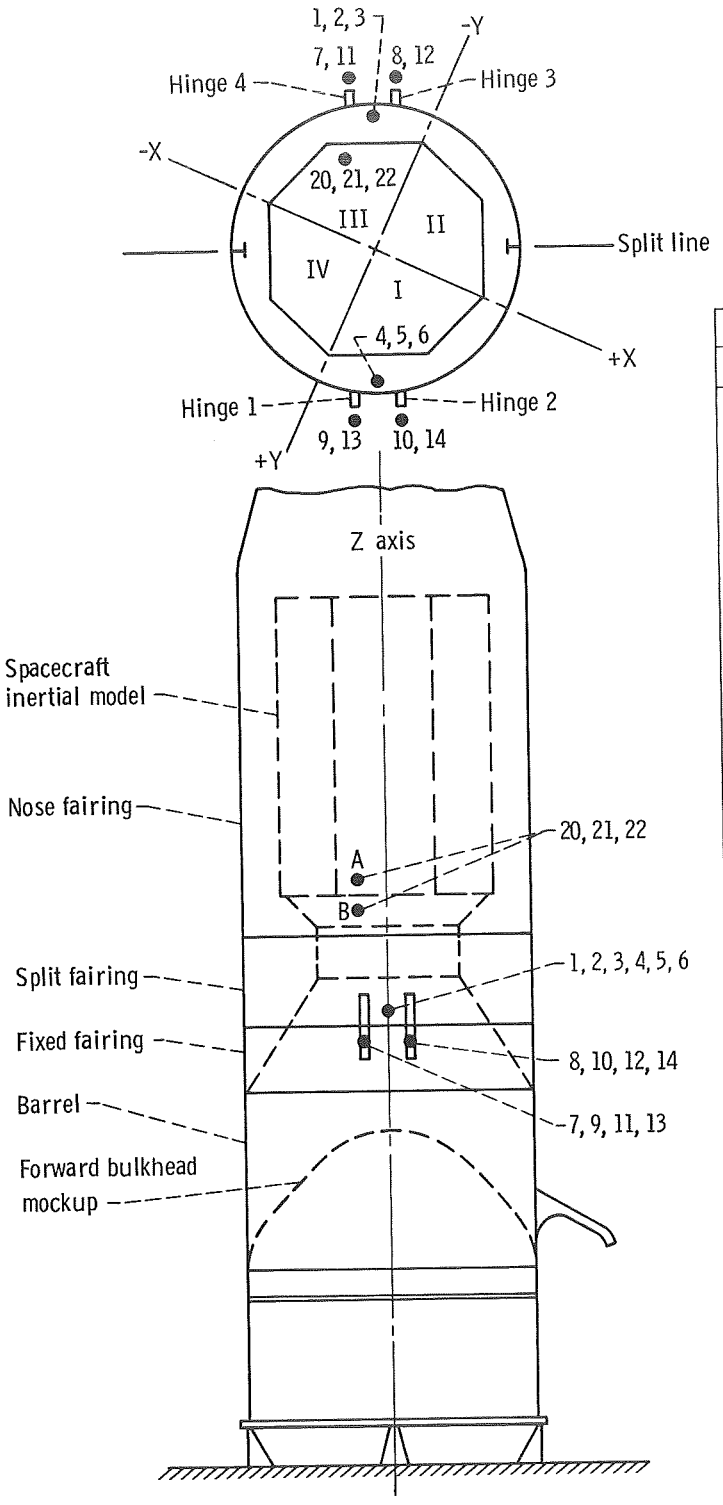

Transducer	
Number	Type
1	Quadrant II-III 15° breakwire
2	Quadrant II-III 45° breakwire
3	Quadrant II-III bus disconnect
4	Quadrant I-IV 15° breakwire
5	Quadrant I-IV 45° breakwire
6	Quadrant I-IV bus disconnect
7	Hinge 1 axial strain gages
8	Hinge 2 axial strain gages
9	Hinge 3 axial strain gages
10	Hinge 4 axial strain gages
11	Hinge 1 radial strain gages
12	Hinge 2 radial strain gages
13	Hinge 3 radial strain gages
14	Hinge 4 radial strain gages
[a]21	Vehicle X-X axis oriented accelerometer
[a]22	Vehicle Y-Y axis oriented accelerometer
[a]23	Vehicle Z-Z axis oriented accelerometer

[a] A - Test 1 location.
B - Tests 2 and 3 location.

(d) Location of electrical transducer type of instruments.

Figure 9. - Concluded.

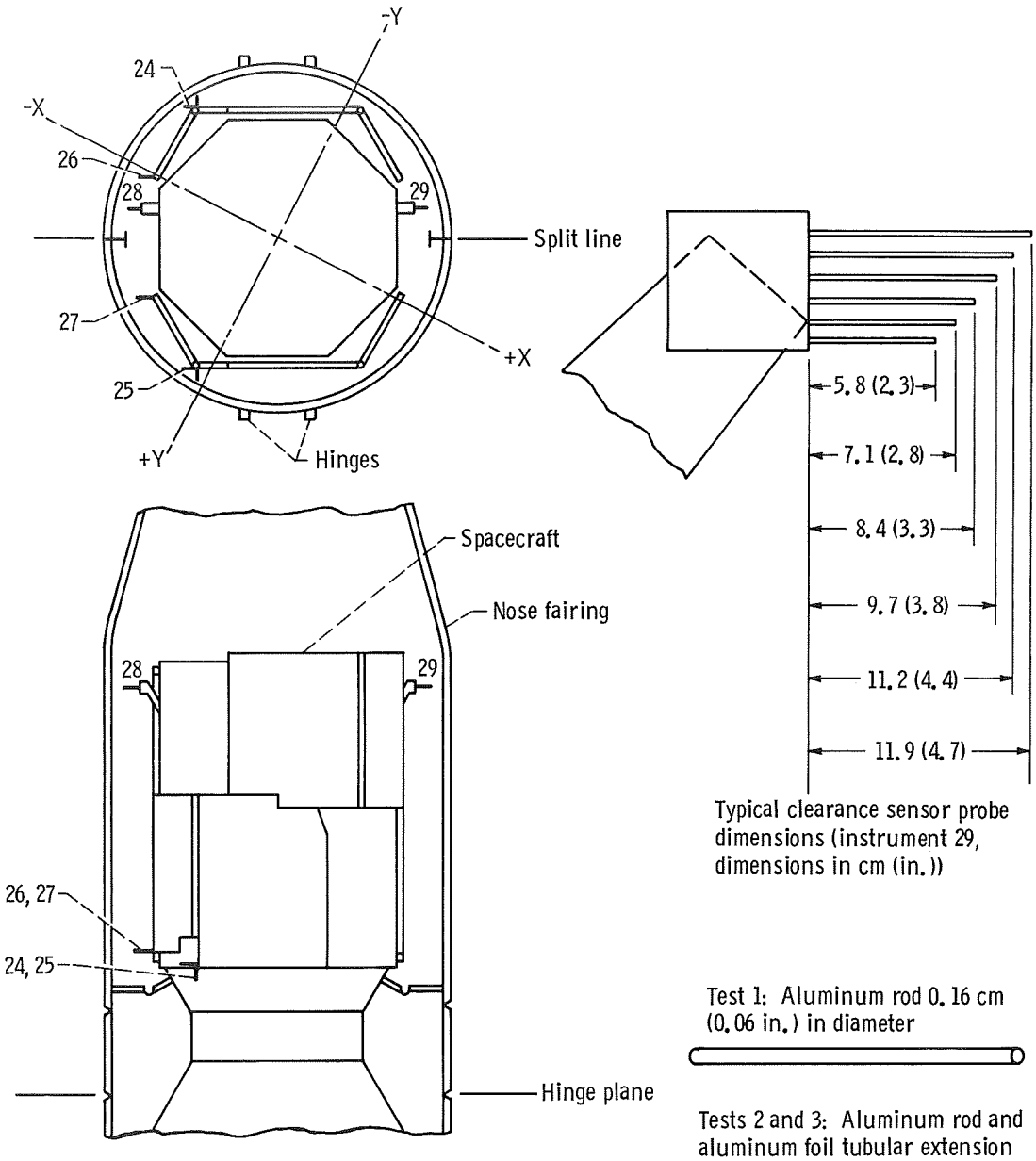

Instrument	Quadrant	Critical clearance components
24	III	Encapsulation bulkhead and main solar panel
25	IV	
26	III	Encapsulation bulkhead and auxiliary solar panel
27	IV	
28	III	Longeron (blast shield) and inertial boom fitting
29	II	

(a) Fairing-spacecraft critical clearance sensors.

Figure 10. - Direct-indicating mechanical sensor instrumentation.

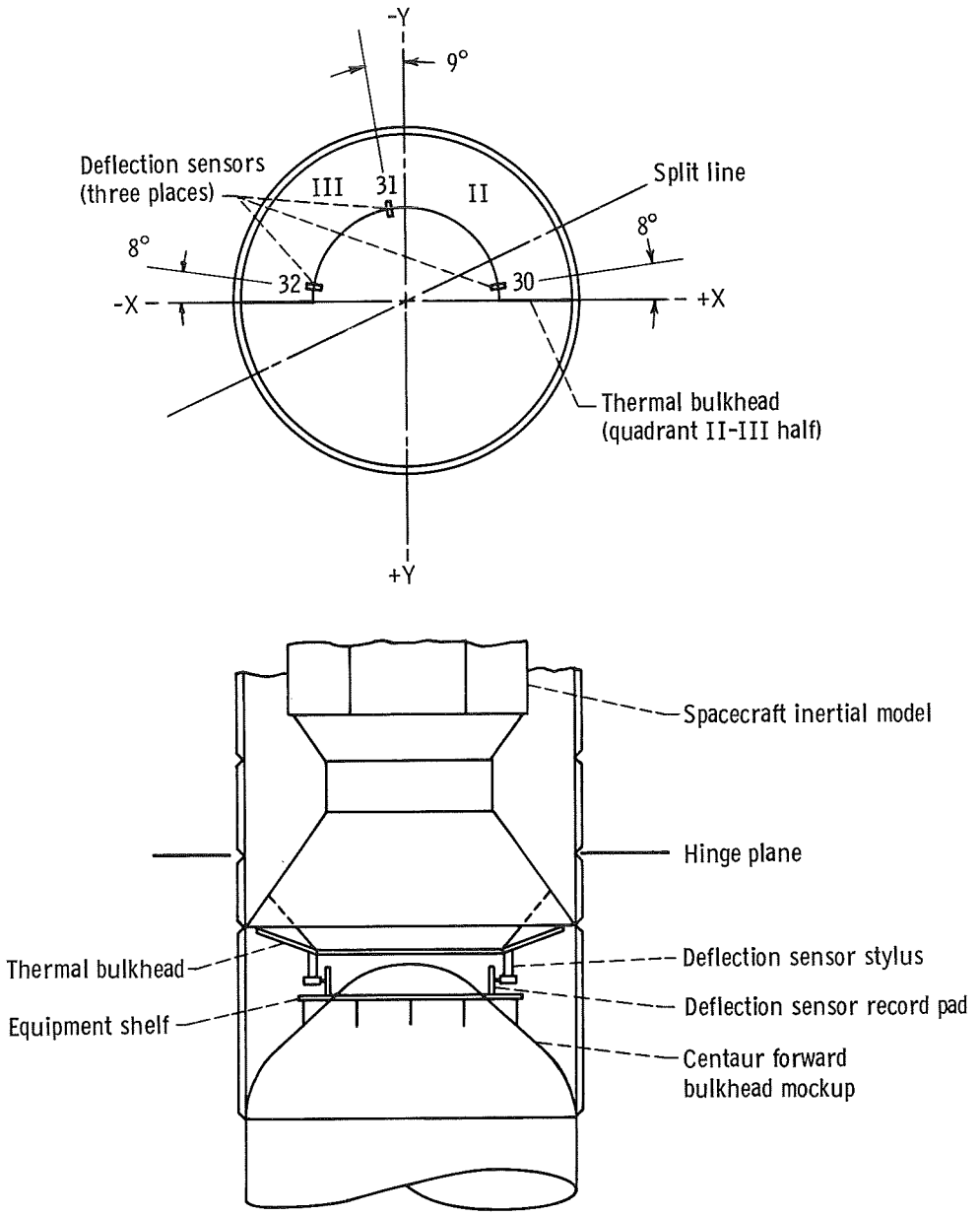

(b) Thermal bulkhead deflection instrumentation.

Figure 10. - Concluded.

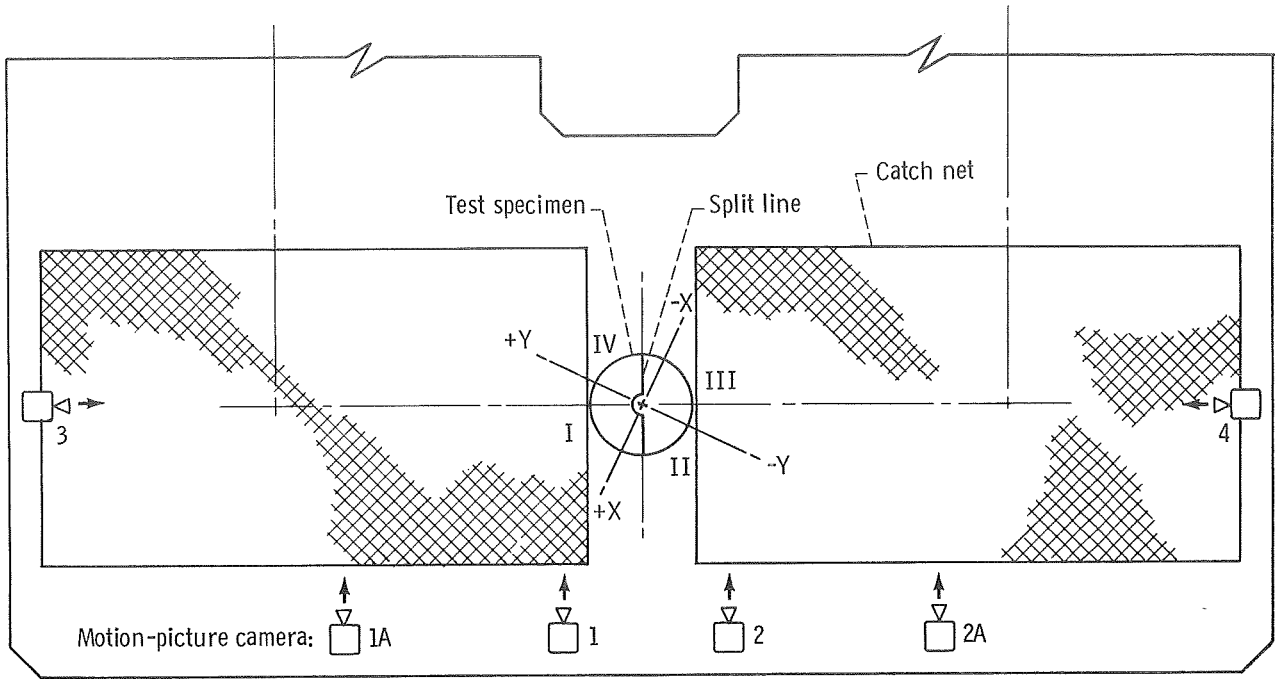

Test chamber plan view

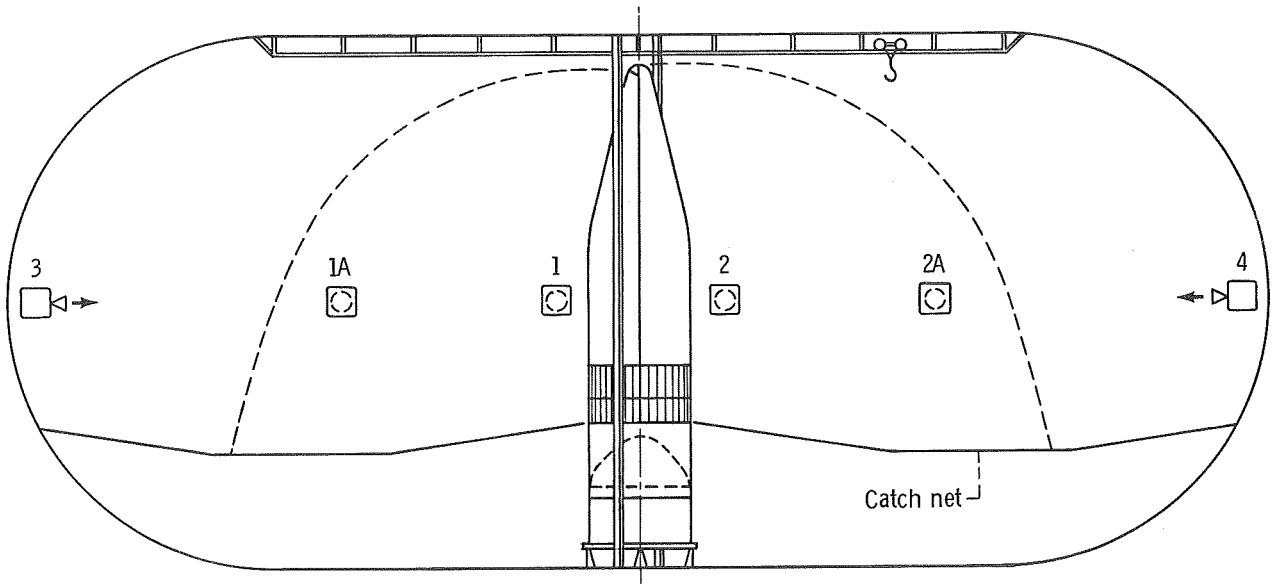

Test chamber section view

(a) General trajectory camera positions.

Figure 11. - Motion-picture camera locations.

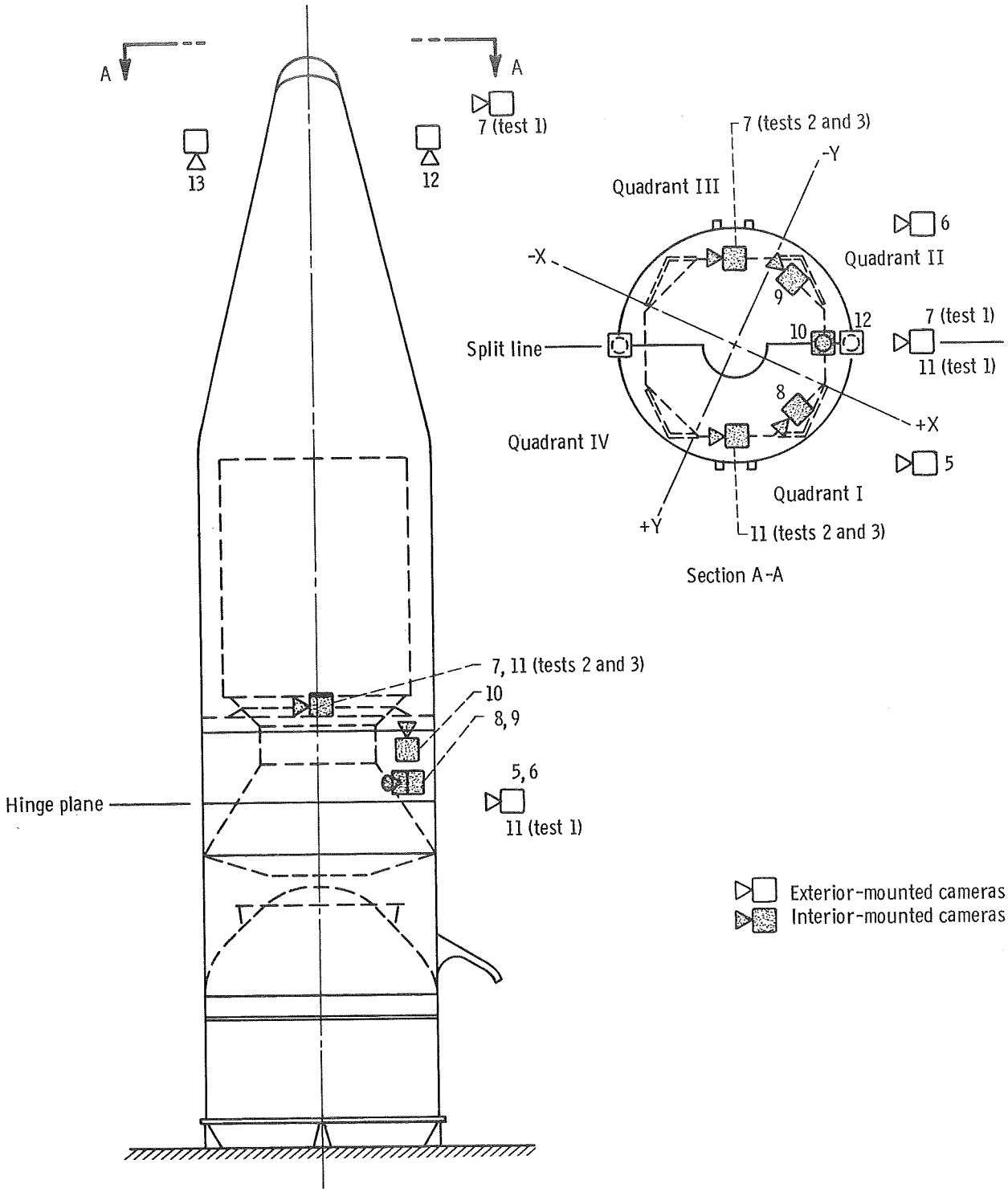

(b) Detail of motion-picture camera positions.

Figure 11. - Continued.

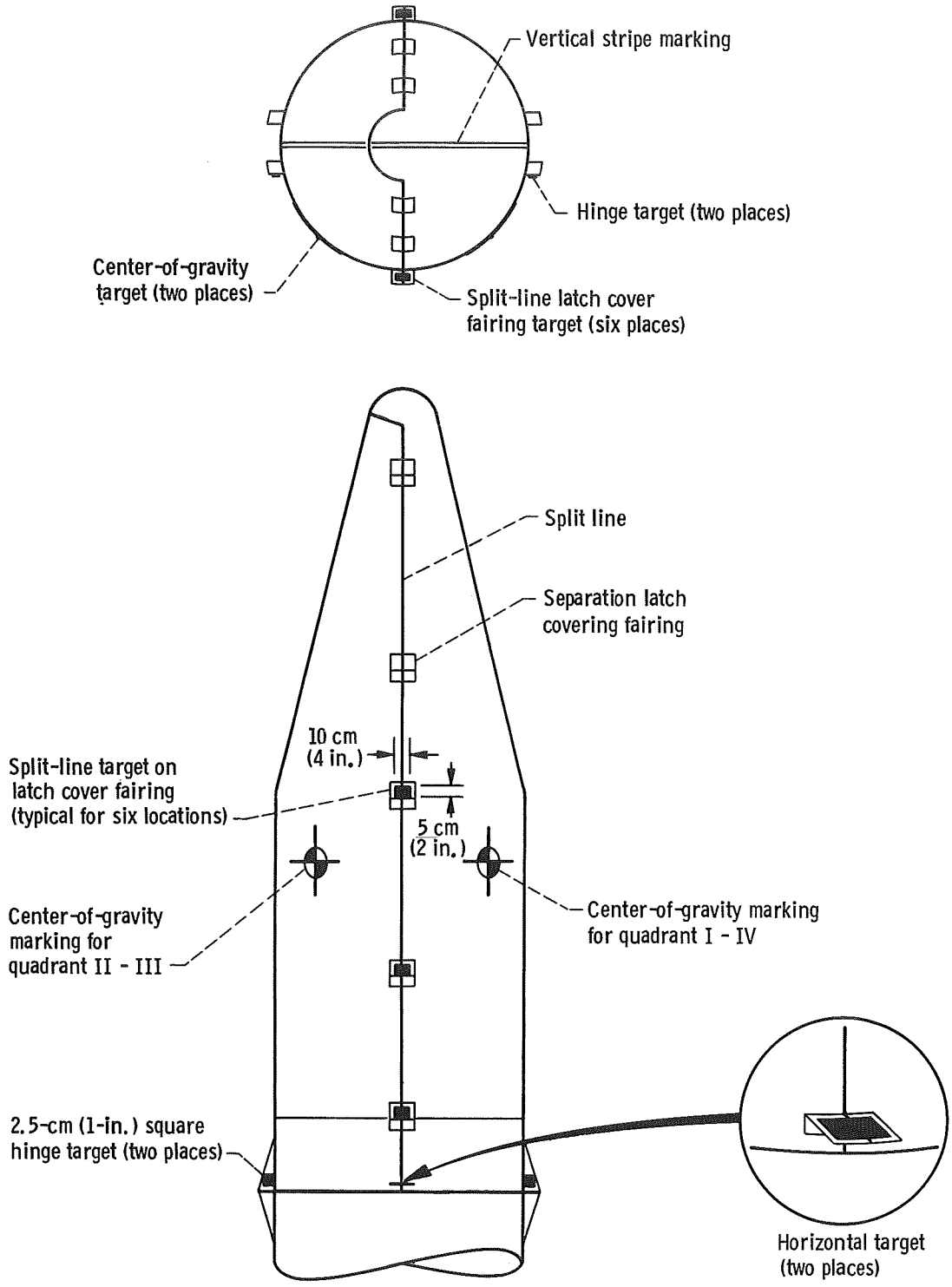

(c) Camera targets and identification marking locations. (Targets and markings, black on white background.)

Figure 11. - Concluded.

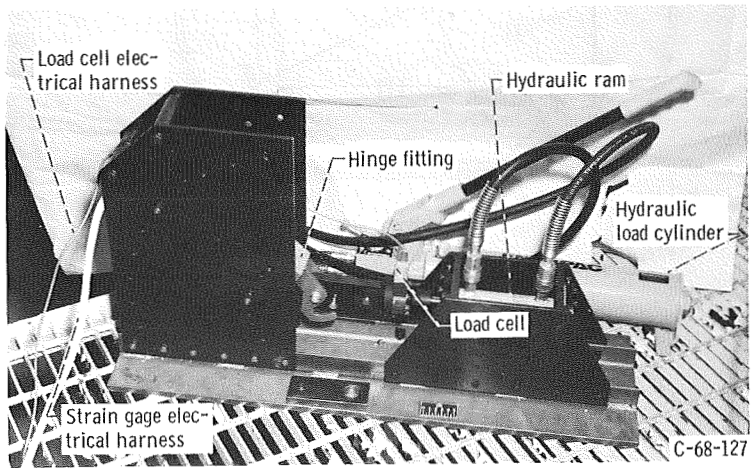

Figure 12. - Hinge fitting calibration fixture.

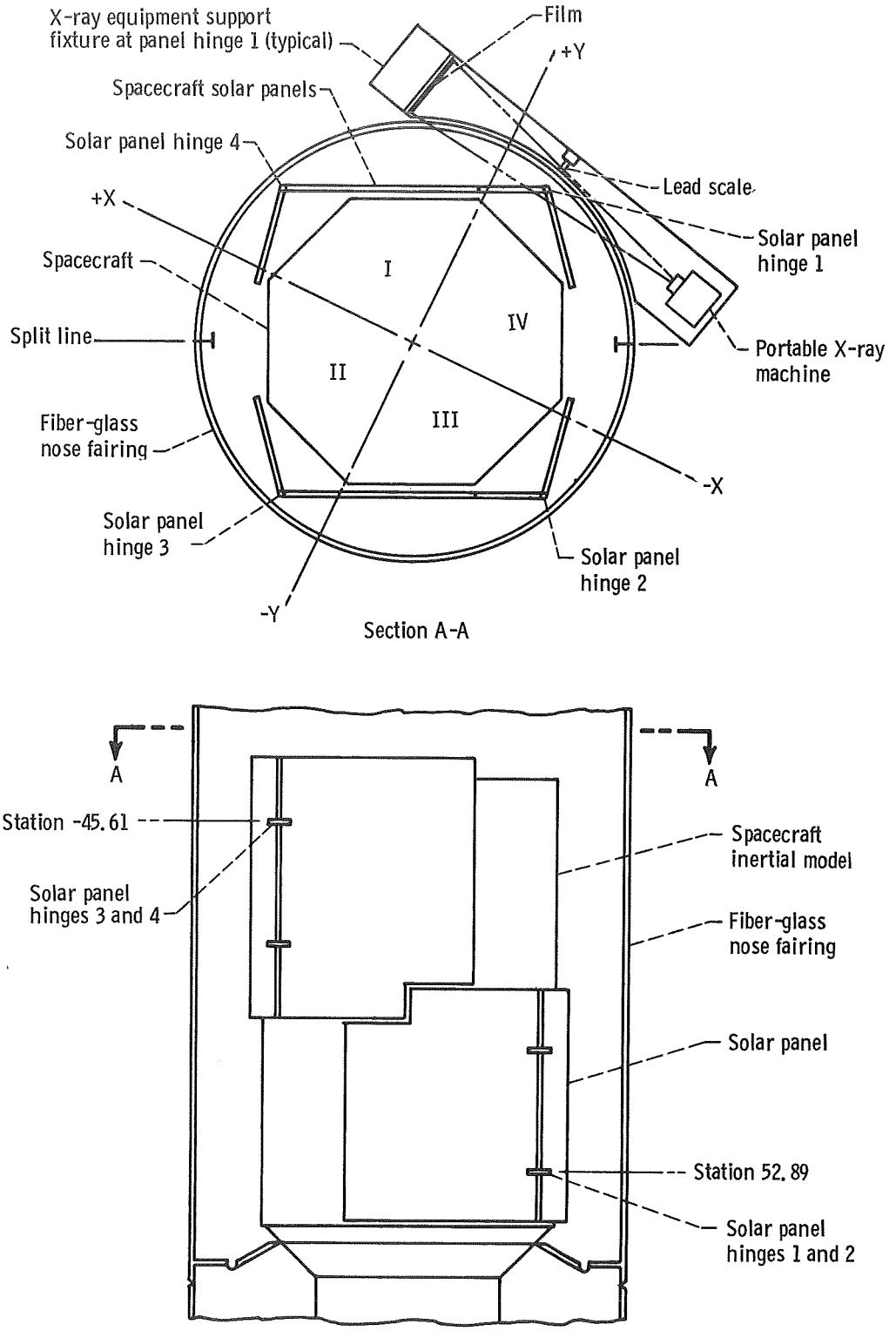

Figure 13. - Radiographic clearance test equipment.

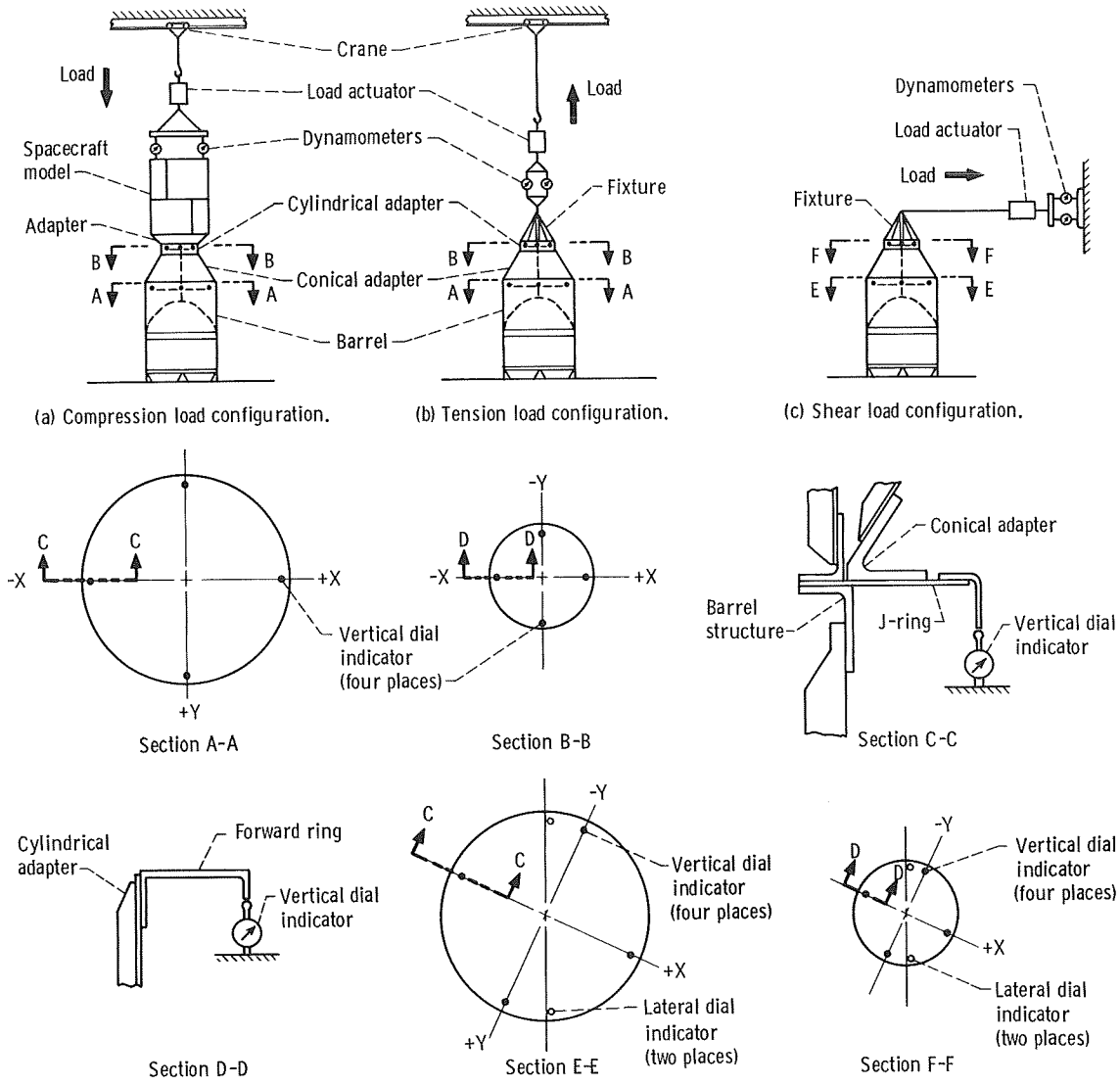

Figure 14. - J-ring deflection test specimen and equipment arrangement.

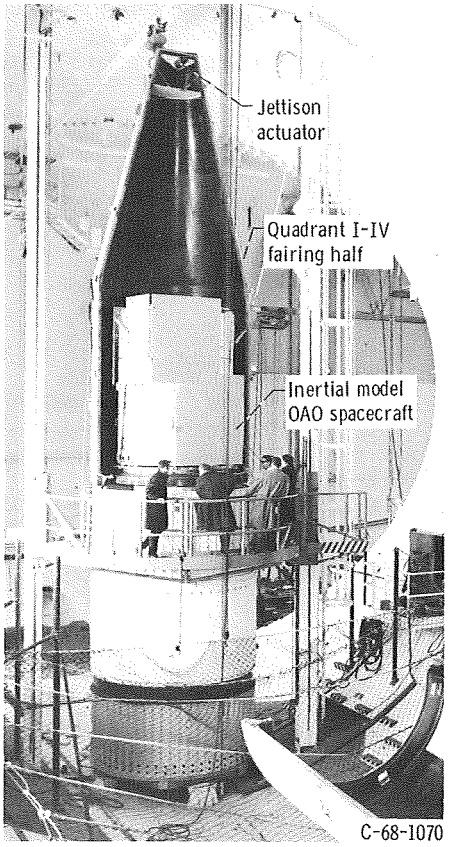

(a) Assembled specimen without quadrant II-III fairing half.

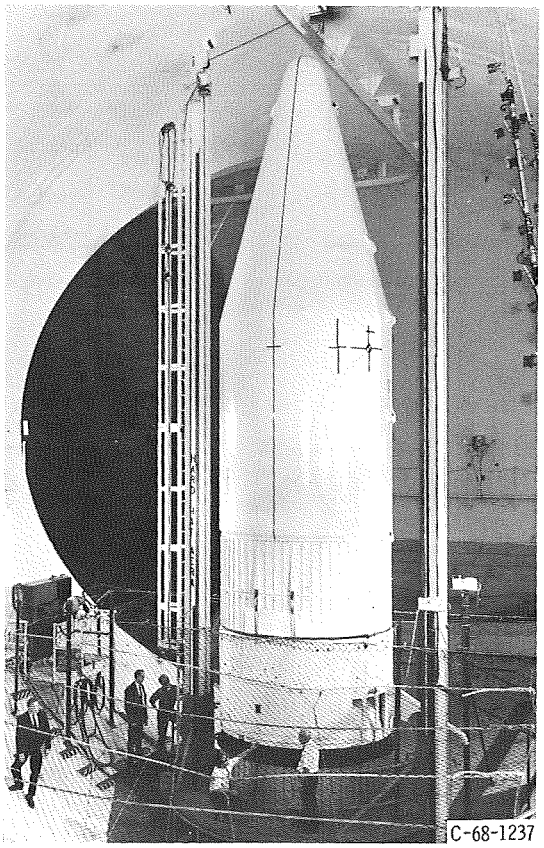

(b) Completely assembled specimen and test equipment.

Figure 15. - Test specimen configuration.

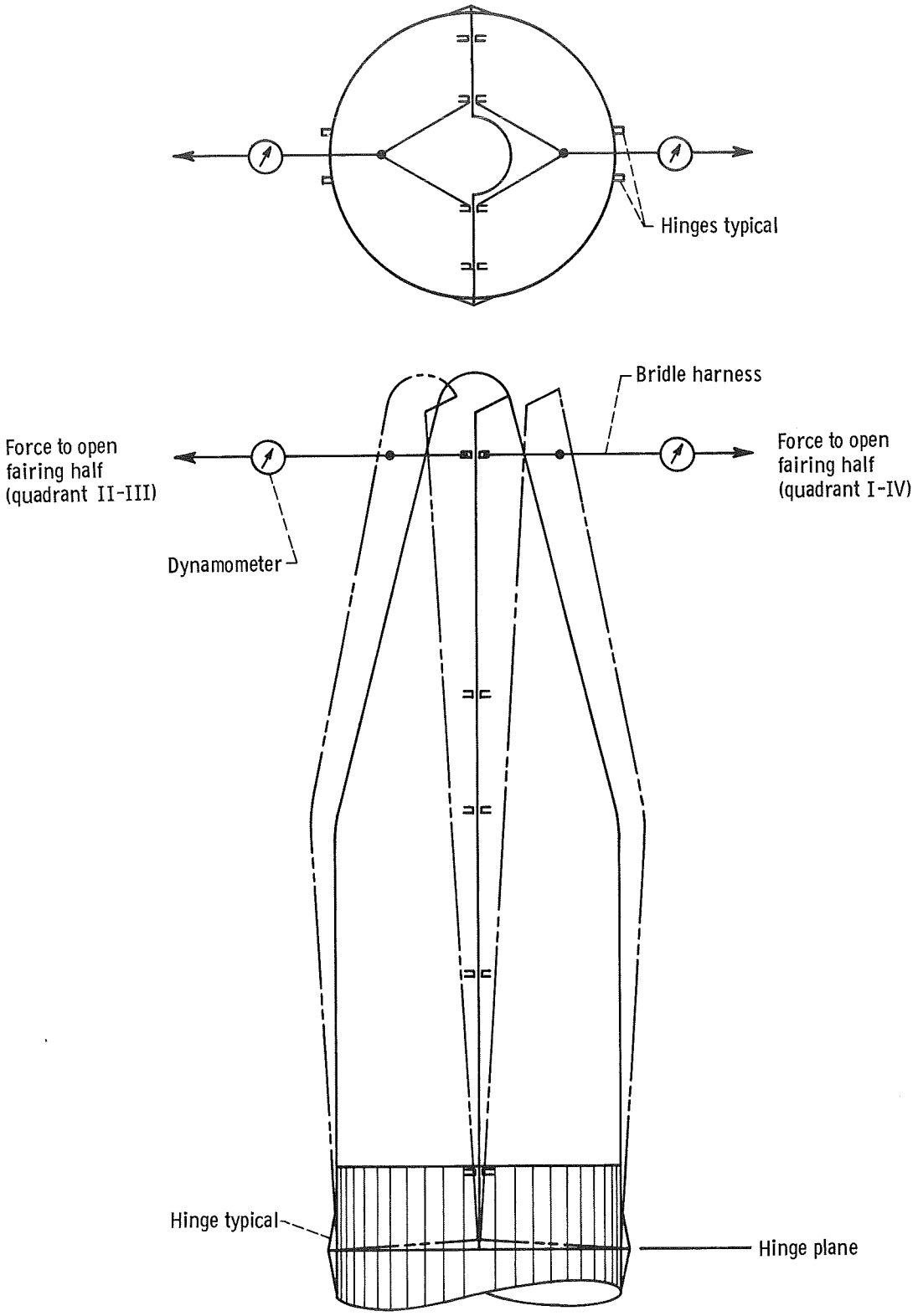

Figure 16. - Separation friction pull test arrangement.

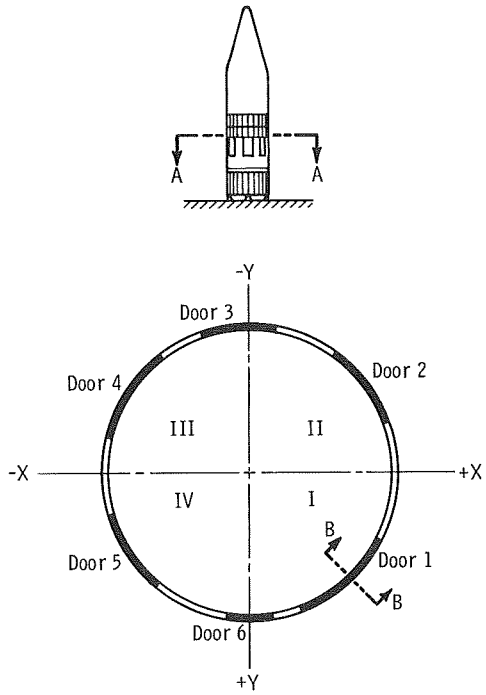

Section A-A

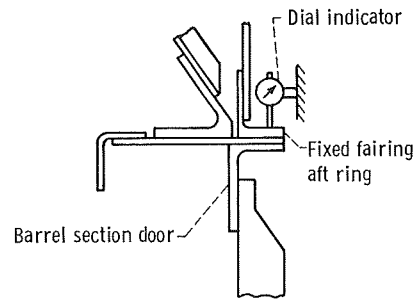

Section B-B (typical for six doors)

Figure 17. - Barrel access door locations and instrumentation.

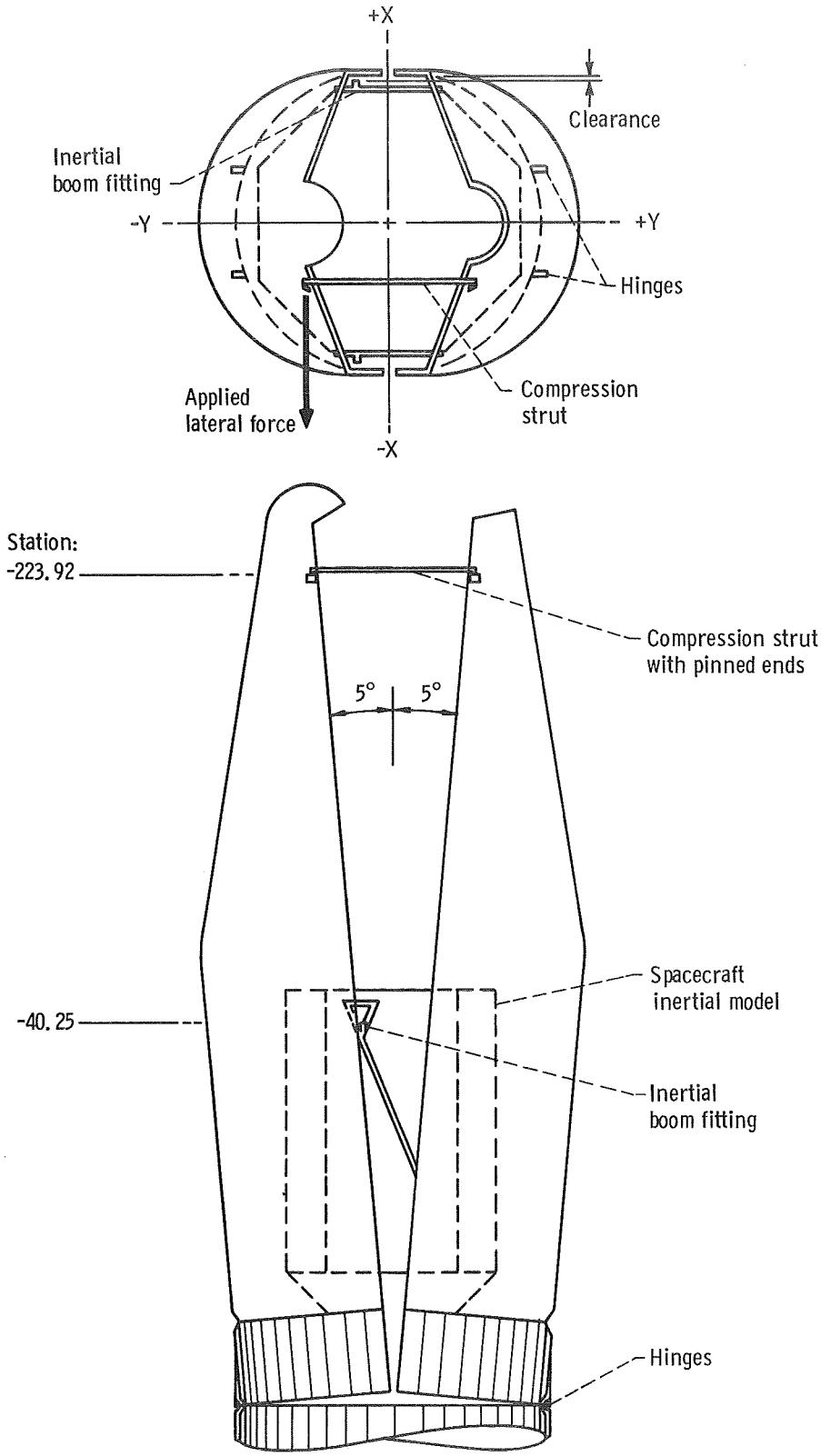

Figure 18. - Rocking dynamics test specimen and equipment setup.

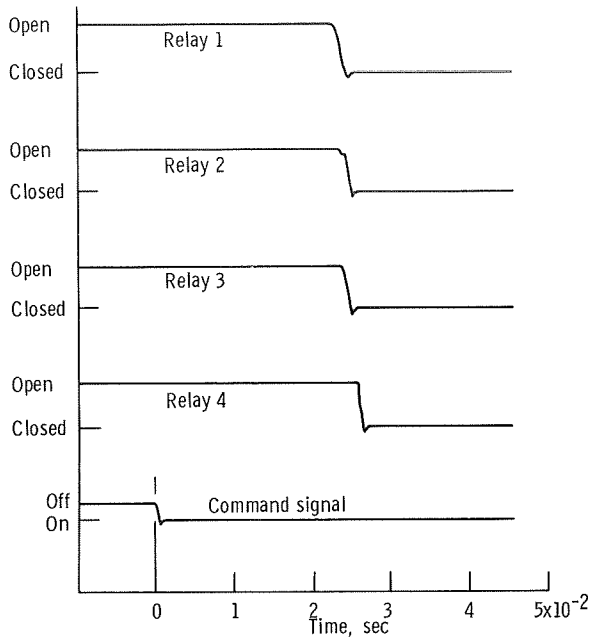

Figure 19. - Pyrotechnic firing system relay operation times.

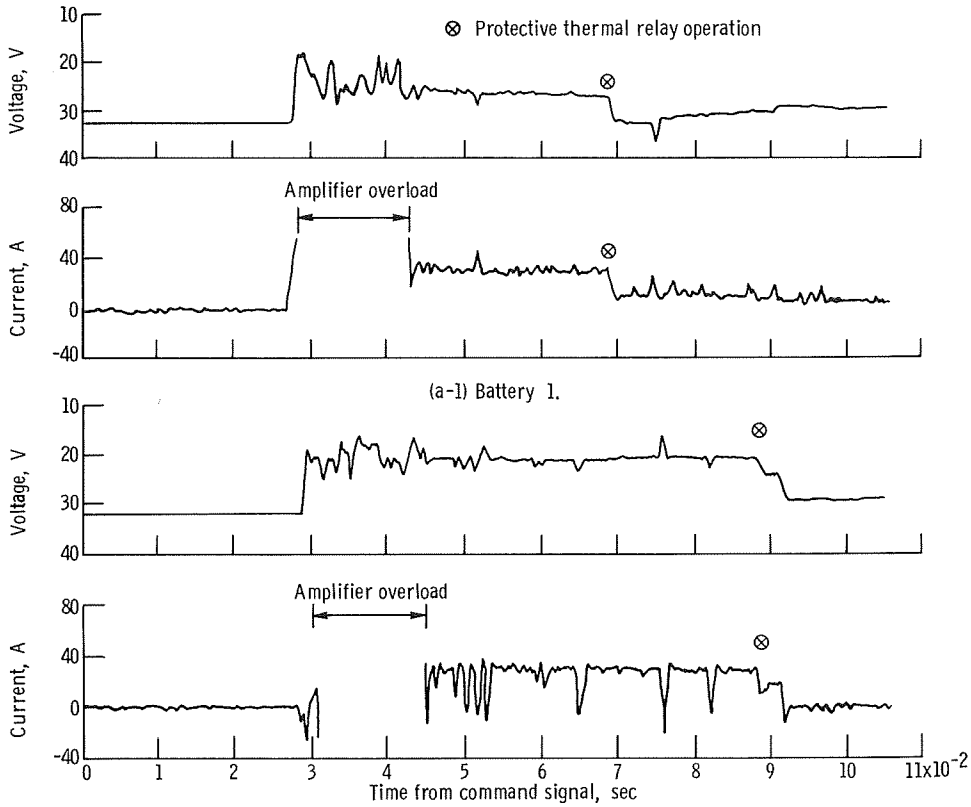

(a) Test 1.

Figure 20. - Pyrotechnic firing circuit battery voltage and amperage.

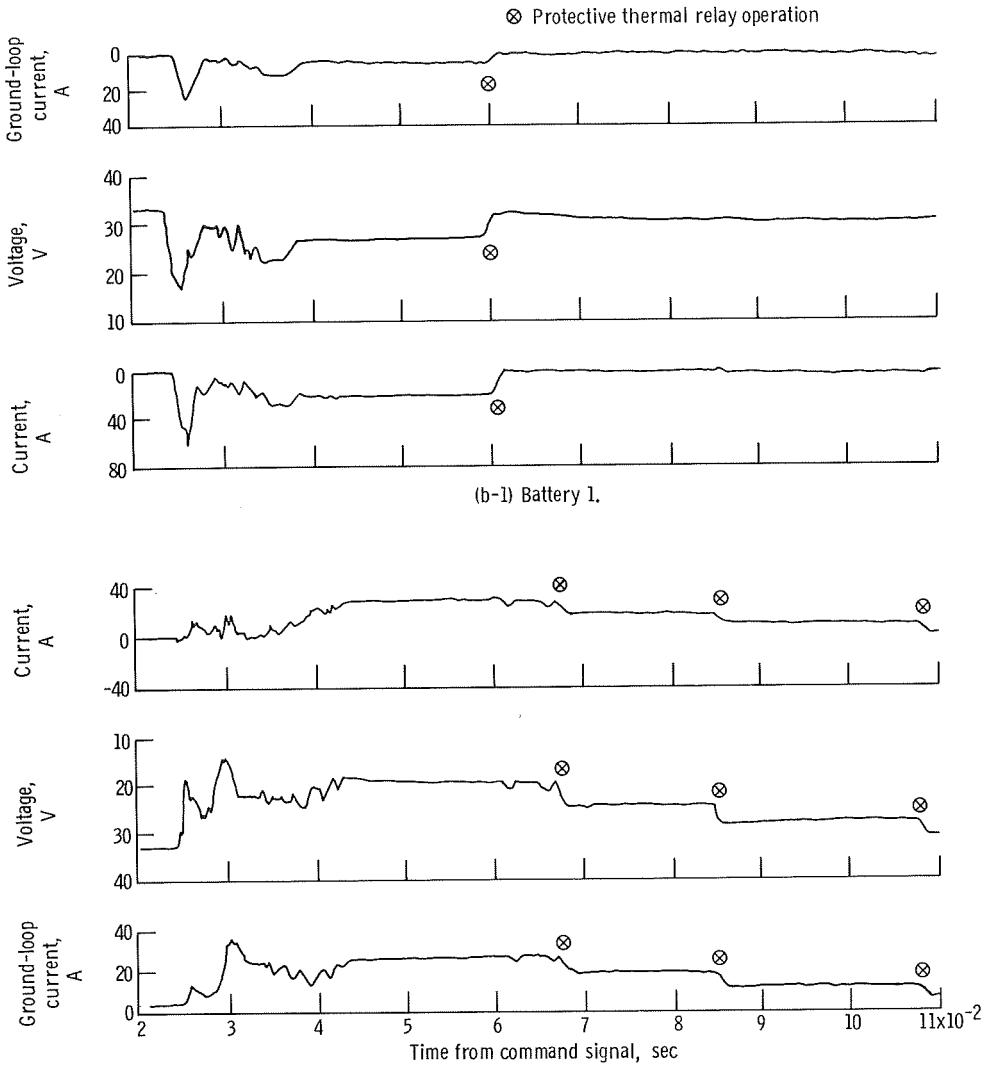

(b-1) Battery 1.

(b-2) Battery 2.

(b) Test 2.

Figure 20. - Continued.

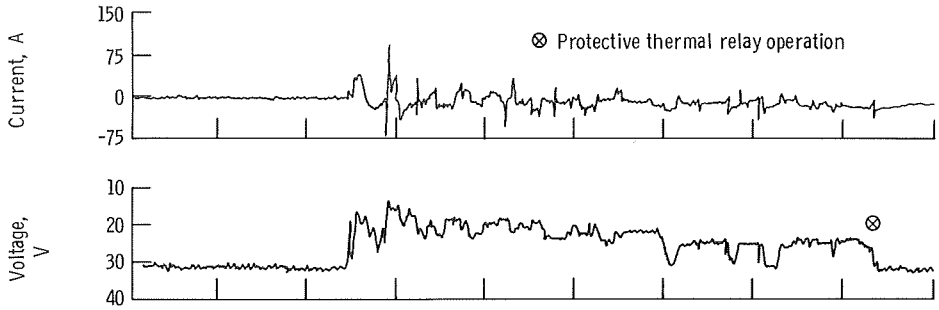

(c-1) Battery 2. Magnetic tape recorded data.

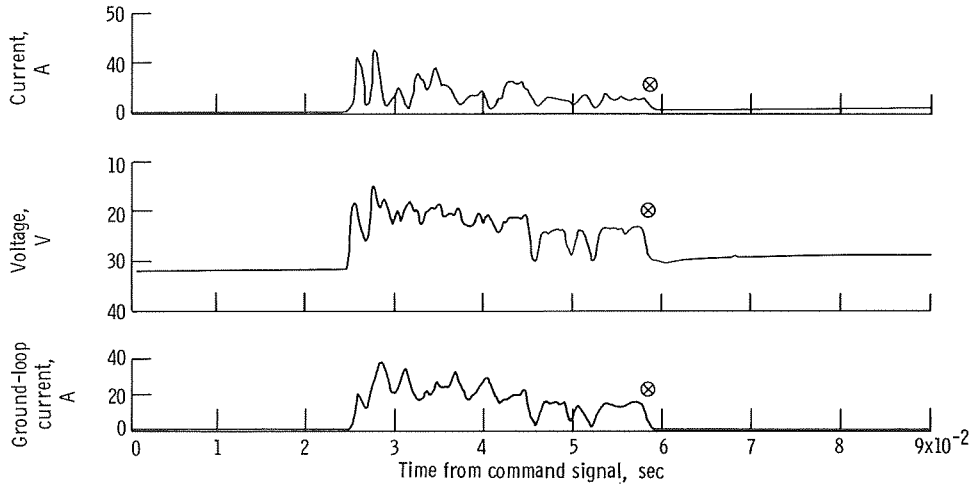

(c-2) Battery 2. Oscillograph recorded data.

(c) Test 3.

Figure 20. - Concluded.

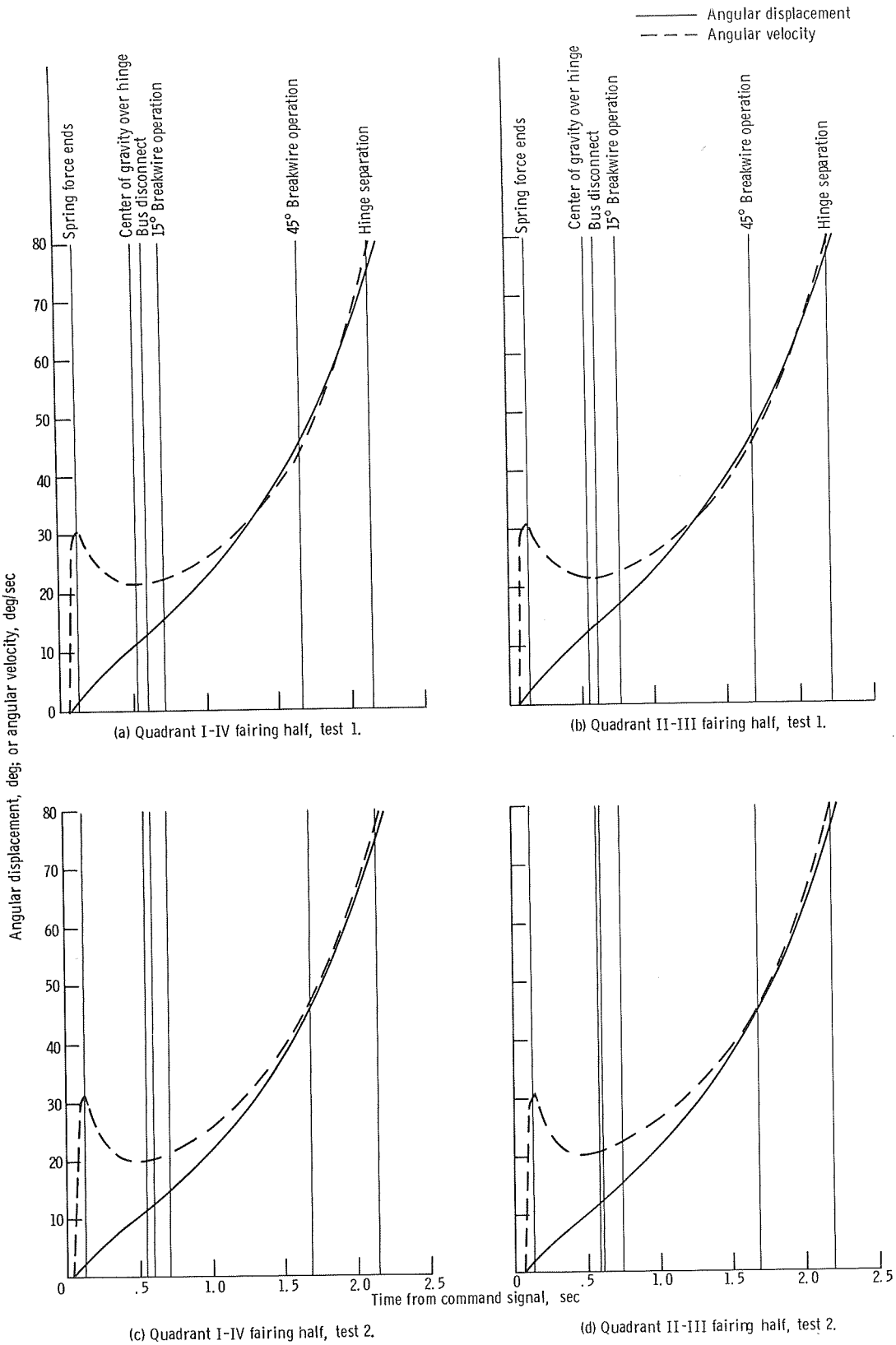

Figure 21. - Nose fairing trajectory characteristics.

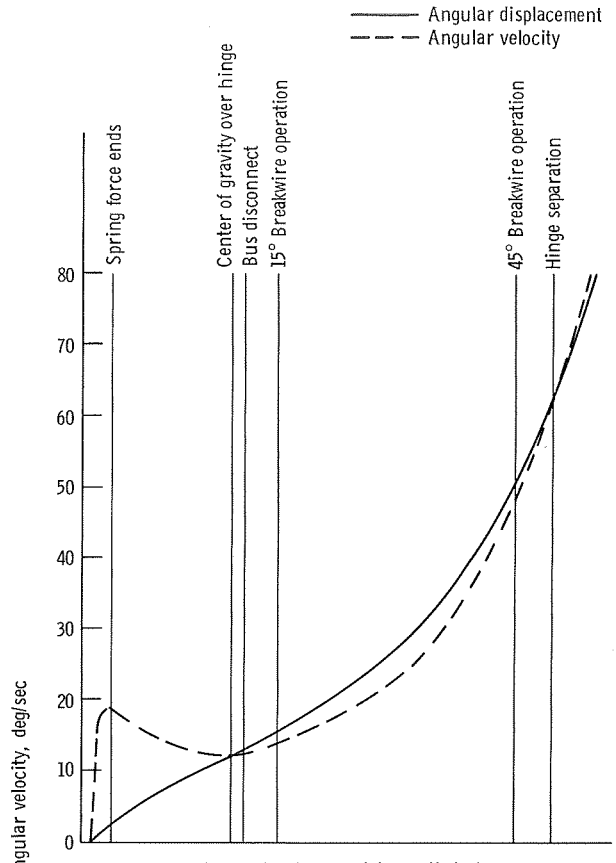

(e) Quadrant I-IV fairing half, test 3.

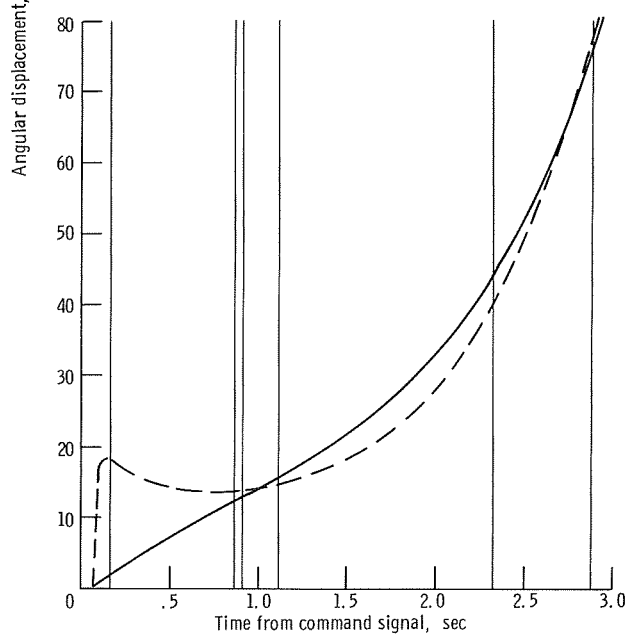

(f) Quadrant II-III fairing half, test 3.

Figure 21. - Concluded.

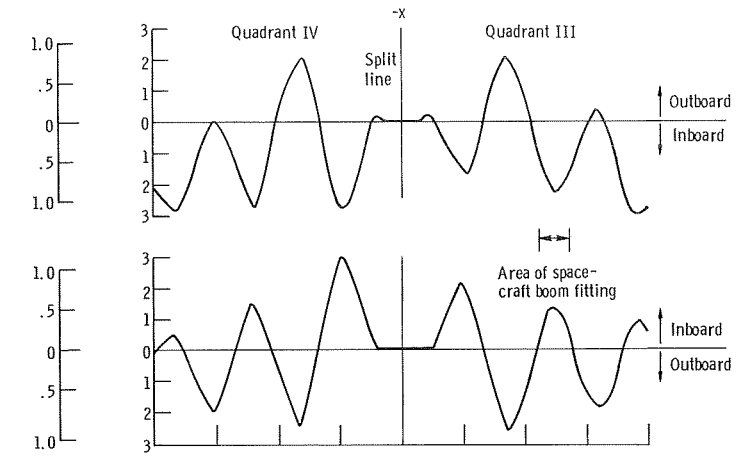

(a) Test 1.

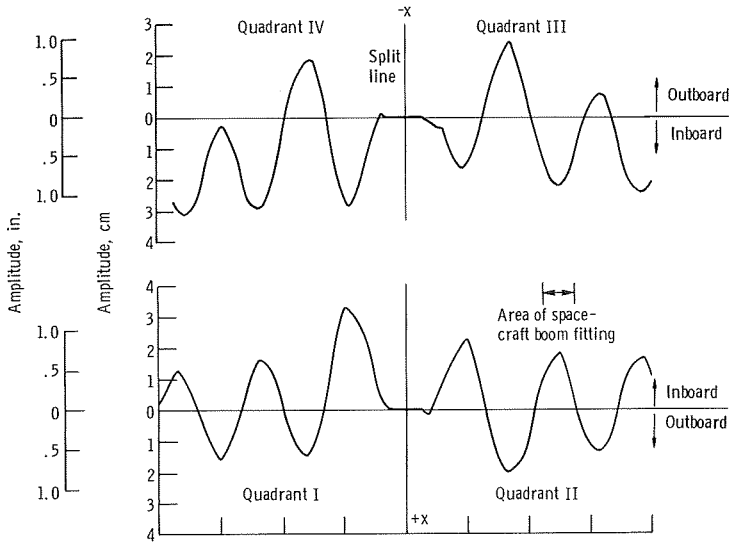

(b) Test 2.

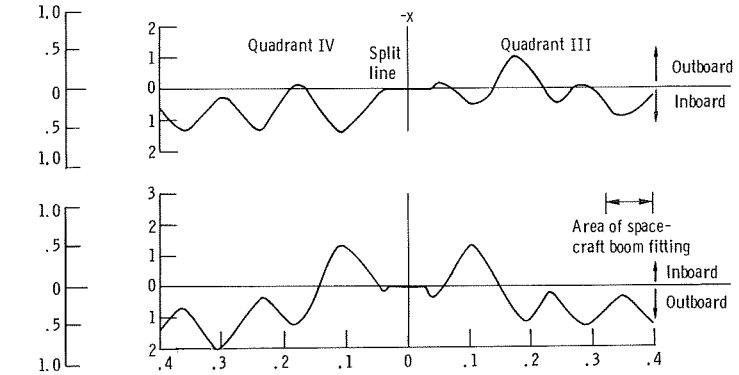

Time from command signal, sec

(c) Test 3.

Figure 22. - Fairing longeron flexing at station -69.

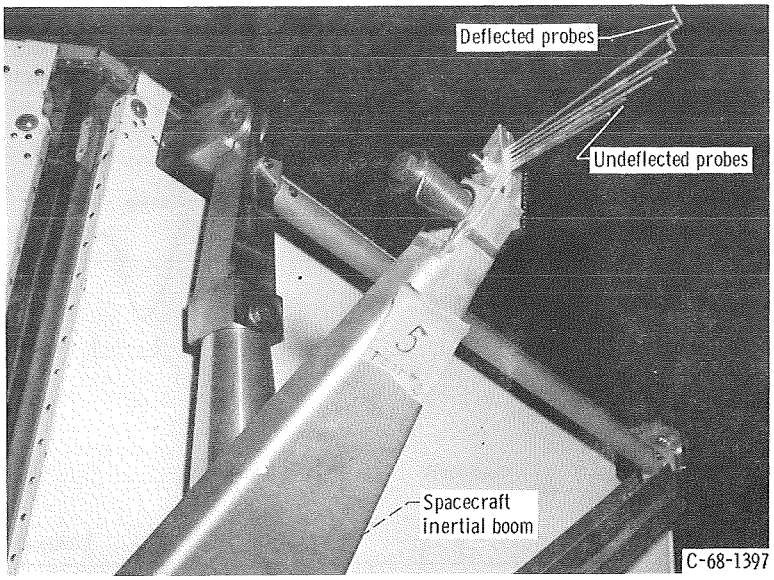

Figure 23. - Typical clearance probe array after test 2.

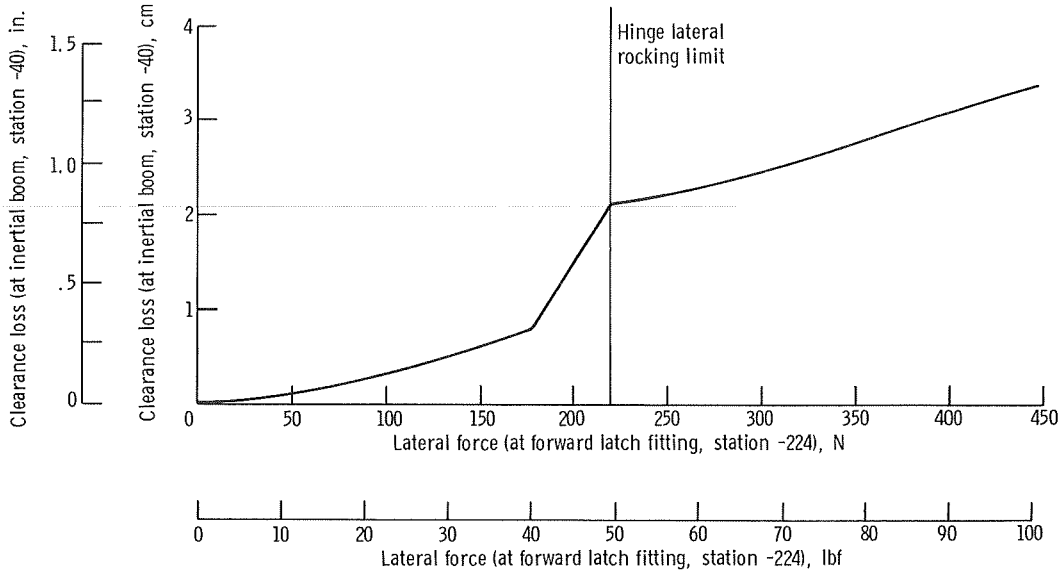

Figure 24. - Quadrant II-III fairing clearance loss from lateral loading.

NASA-Langley, 1970 —— 31 E-5673

NATIONAL AERONAUTICS AND SPACE ADMINISTRATION
WASHINGTON, D. C. 20546

OFFICIAL BUSINESS

FIRST CLASS MAIL

POSTAGE AND FEES PAID
NATIONAL AERONAUTICS A
SPACE ADMINISTRATION

POSTMASTER: If Undeliverable (Section 15
Postal Manual) Do Not Retu

"The aeronautical and space activities of the United States shall be conducted so as to contribute . . . to the expansion of human knowledge of phenomena in the atmosphere and space. The Administration shall provide for the widest practicable and appropriate dissemination of information concerning its activities and the results thereof."

—NATIONAL AERONAUTICS AND SPACE ACT OF 1958

NASA SCIENTIFIC AND TECHNICAL PUBLICATIONS

TECHNICAL REPORTS: Scientific and technical information considered important, complete, and a lasting contribution to existing knowledge.

TECHNICAL NOTES: Information less broad in scope but nevertheless of importance as a contribution to existing knowledge.

TECHNICAL MEMORANDUMS: Information receiving limited distribution because of preliminary data, security classification, or other reasons.

CONTRACTOR REPORTS: Scientific and technical information generated under a NASA contract or grant and considered an important contribution to existing knowledge.

TECHNICAL TRANSLATIONS: Information published in a foreign language considered to merit NASA distribution in English.

SPECIAL PUBLICATIONS: Information derived from or of value to NASA activities. Publications include conference proceedings, monographs, data compilations, handbooks, sourcebooks, and special bibliographies.

TECHNOLOGY UTILIZATION PUBLICATIONS: Information on technology used by NASA that may be of particular interest in commercial and other non-aerospace applications. Publications include Tech Briefs, Technology Utilization Reports and Notes, and Technology Surveys.

Details on the availability of these publications may be obtained from:

SCIENTIFIC AND TECHNICAL INFORMATION DIVISION

NATIONAL AERONAUTICS AND SPACE ADMINISTRATION

Washington, D.C. 20546